NTNU

Norwegian University of
Science and Technology

Contribution of humidity and pressure to PEMFC performance and durability

Jan Gregor Høydahl Sørli

Master of Science in Energy and Environment

Submission date: June 2008

Supervisor: Gernot Krammer, EPT

Co-supervisor: Thor Anders Aarhaug, SINTEF Materialer og kjemi
Steffen Møller-Holst, SINTEF Materialer og kjemi

Norwegian University of Science and Technology
Department of Energy and Process Engineering

Problem Description

Experimental study of the effect of clamping pressure, gas humidification and back pressure to PEMFC performance and durability. The methodology aims to quantify the contribution from the input variables as well as give indication of the optimal conditions for both performance and durability for the variable spaces used.

The following questions should be considered in this work:

1. Which experimental methods allow the investigation of durability of PEMFC?
2. Why are clamping pressure, gas humidity and back pressure relevant when considering durability and performance?
3. How do the operating conditions affect durability?
4. What is the correlation between lifetime and performance?
5. Which are the criteria for optimal PEMFC operation?

Assignment given: 21. January 2008
Supervisor: Gernot Krammer, EPT

Declaration

I hereby declare that this thesis is written independently and in accordance with the examination regulations of The Norwegian University of Science and Technology.

Trondheim, 11.06.08

Jan Gregor Høydahl Sørli

Preface

This report is a result of my master thesis carried out at SINTEF Materials and Chemistry. This master thesis is also the last part of my Master of Science and Technology degree at NTNU.

First of all, I would like to express my gratitude to the employees at SINTEF Materials and Chemistry for giving me the opportunity to complete my studies and to work with fantastic people. Special thanks to Thor Anders Aarhaug, Steffen Møller-Holst, Magnus Skinlo Thomassen and Axel Baumann Ofstad for sharing their unique knowledge on fuel cells, being helpful and encouraging. Looking back on the five years at NTNU the last year working on my project work and master thesis at SINTEF has been my best in every respect.

I would also like to thank my supervisor at NTNU, Professor Gernot Krammer for valuable discussions throughout the master thesis.

Trondheim 11.06.08

Jan Gregor Høydahl Sørli

Abstract

In this work, a 2^{3-1} designed experiment has been performed to evaluate the effect of selected operating conditions on PEMFC performance and durability. Relative humidity, clamping pressure and back pressure were studied at two levels for Gore MEAs and GDLs. Two replicated experiments were performed. An ON/OFF test cycle was used to accelerate degradation. Total duration of the tests, after a break in procedure suggested by Gore, was ten days. In addition to sampling of voltage and current response and ohmic resistance, effluents were manually sampled from both electrodes every 24 hours and analyzed.

Experiments with low humidification levels showed inferior durability. The combination of high relative humidity (100 %), high clamping pressure (10 barg) and high back pressure (1.5barg) result in the best performance and the lowest degradation rate. Results indicate that relative humidity is important both for performance and durability.

Generally, fluoride emission rates (FER) showed an increasing trend with time. Higher rates were observed at the cathode. For the experiment with low relative humidity (25 %), low clamping pressure (5 barg) and high back pressure (1.5 barg) FER was significantly higher compared to the other experiments.

For all tests the sulfur emission rates (SER) are initial high. Rates are higher at the anode. For the experiment with high relative humidity, low clamping pressure and no back pressure, the SER was significantly higher than for the other experiments. The sustained high levels of sulfur are probably a result of sulfuric acid residue from production of the MEA and/or GDL. High humidification of gases appears to more effectively wash out the sulfur.

Contents

Nomenclature

Latin symbols

e^-	Electron
E	EMF, [V]
E^0	EMF at standard temperature and pressure, and with pure reactants, [V]
F	Faraday constant, the charge on one mole of electrons, 96485 [Coulomb]
i	Current density, [A cm^{-2}]
n	Number of cells in a fuel cell stack or number of moles
P	Total pressure, [Pa]
p_i	Partial pressure of gas i, [Pa]
R	Universal gas constant, 8.314 [J K^{-1} mol^{-1}], also electrical resistance [ohm cm^{-2}]
T	Temperature, [K]
V	Voltage, [V]
V_a	Activation overvoltage, [V]
V_c	Average voltage of one cell in a stack, [V]
V_r	Ohmic overvoltage, [V]
ΔG	Change in Gibbs free energy, [J mol^{-1}]
ΔH	Change of enthalpy, [J mol^{-1}]

Greek symbols

Δ	Arithmetic difference
η	Efficiency and overpotential (non-ohmic)
λ	Stoichiometry factor

Abbreviations, definitions

Anode	The electrical conductor of a device that electrons flow out of
barg	Gauge pressure, overpressure
Cathode	The electrical conductor of a device in which electrons flow into
C	Carbon
EMF	Electromotive force, [V]
FER	Fluoride Emission Rate, [ng h^{-1} cm^{-2}]
GDL	Gas Diffusion Layer
MEA	Membrane Electrode Assembly
OCV	Open circuit voltage, [V]
lN	Normal liter, [0°C,1 atm]
iR	Ohmic loss, [V]
PEM	Proton Exchange Membrane or Polymer Electrolyte Membrane
PEMFC	Proton Exchange Membrane Fuel Cell
PSFA	Perfluorinated sulfonic acid
Pt	Platinum
RHE	Reversible Hydrogen
Ru	Ruthenium
SER	Sulfate Emission Rate, [ng h^{-1} cm^{-2}]
STD	Standard Deviation

1 Introduction

The main incentive for establishing a hydrogen oriented economy is the reduction of local emissions, improving security of energy supply and reduction of greenhouse gas emissions. Due to the growing concerns about the urban air quality and global climate change, fuel cell technology has attracted great attention. Proton exchange membrane fuel cells (PEMFCs) have the potential to solve some of the problems associated with future production and consumption of energy. Supplied with hydrogen derived from renewable energy sources, fuel cells could positively influence several areas, including environmental, economic and energy security.

Automobile manufacturers and fuel cell developers have produced PEMFCs for many years. There are, however, two major still remaining challenges that have to be solved prior full scale commercialization: cost and lifetime. One of the most important factors limiting the lifetime of PEMFCs is MEA degradation.

To improve durability of PEMFC without increasing cost or loosing performance the factors that determine a PEMFCs lifetime need to be studied further. Studies have shown that several factors can reduce PEMFC lifetime, including choice of materials, material composition and operating conditions. Important operational conditions that affect performance and lifetime include fuel cell temperature, voltage and current, humidity, pressures and impurities in the oxidant or fuel stream.

In order to meet the requirements for the automotive applications, MEA used in PEMFC will be required to demonstrate durability of about 5000 hours (2010 target) under normal automotive operating conditions [1]. Membranes must be able to perform over the full range of system operating temperatures with less than 5% performance loss at the end of life [1]. Key to achieving the lifetime targets will be the durability of the MEA. Degradation rate requirements are normally based on beginning-of-life performance, end-of-life performance requirements and durability requirements in terms of operating hours.

Even when operating with high purity hydrogen, today's PEMFCs have unsatisfactory lifetime. It has been shown that durability of PEMFCs using Nafion® 120 reached 60,000 hours of continuous fuel cell operation. However, due to increased demands for maximizing performance efficiency and lowering ohmic losses of PEMFC, durability has been reported in the range of a few thousand (for car applications) to several tens of thousands hours (for stationary applications) depending on the chosen operating conditions.

When considering the issue of optimal PEMFC operation there are several factors that have to be considered. The optimal operation will differ for different applications and will be an optimum balance of cost, efficiency, reliability and durability.

The rate of degradation is a function of the operating conditions, and loss in performance could be due to both electrode and membrane degradation. Finding a correlation between

different operating conditions could be useful in further work to better understand membrane degradation.

This thesis aims to quantify the effect of chosen operating condition on PEMFC performance and durability. The effect will be experimentally studied on a single PEMFC test cell. The operating conditions that will be studied are clamping pressure, gas humidification and back pressure. The experiments will use in situ measurements to evaluate different loss mechanisms.

1.1 Outline of thesis

Each chapter starts by shortly stating the purpose and content of the chapter. Information which is unessential for the context is placed in appendices. Most of the results from the experimental tests are reported in figures and tables. References are numbered in the reference list and are shown as brackets in the text.

Chapter 2 gives a short theoretical description of PEMFC. In addition different mechanisms that affect fuel cell performance and lifetime are addressed.

In Chapter 3 different PEMFC durability testing methods are addressed. Chapter 4 describes the methodology used in this thesis.

In Chapter 5 the experimental setup is described. Some introductory experiments used to set define variable space are reported.

Chapter 6 contains a description of the test procedure used. In Chapter 7 results from the experiments are discussed.

An overall conclusion of the experimental work is drawn in Chapter 8.

2 Theoretical background of PEMFC

2.1 Structure and reactions

In a PEMFC, two half-cell reactions take place simultaneously, an oxidation reaction (loss of electrons) at the anode and a reduction reaction (gain of electrons) at the cathode. The membrane electrode assembly (MEA) consists of two electrodes, the anode and the cathode, separated by a proton exchange membrane (PEM). A gas diffusion layer (GDL) is used at each electrode to facilitate gas distribution. A schematic cross section of a single PEMFC showing the different components and the reactions taking place is shown in Figure 1.

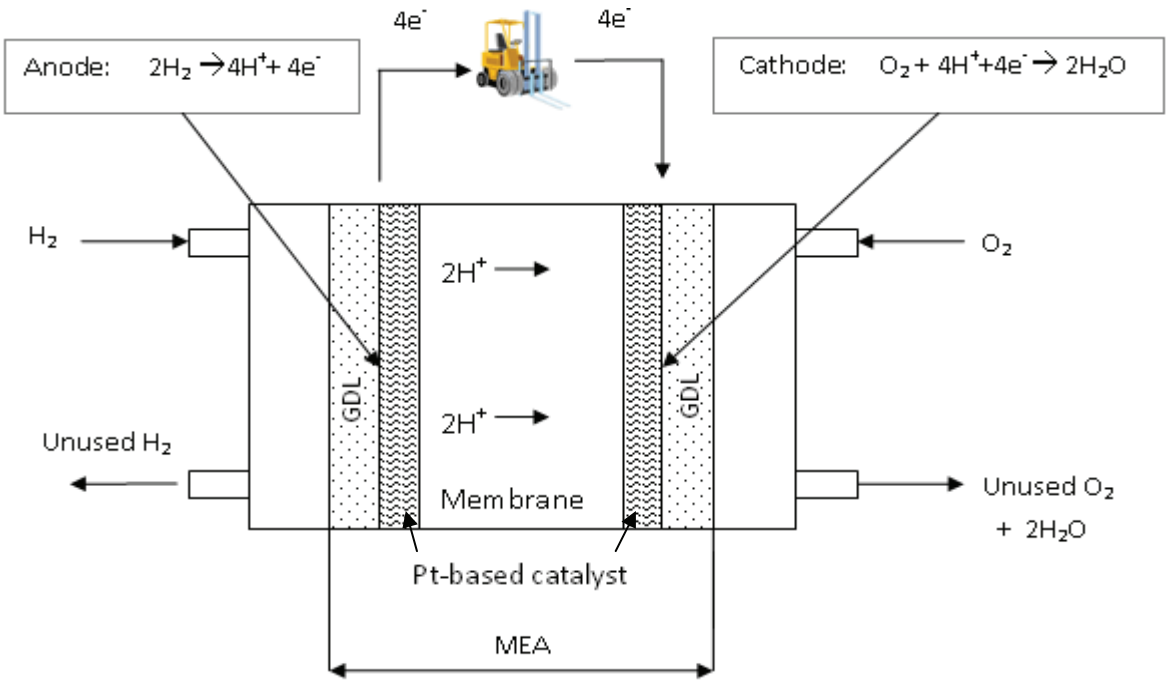

Figure 1 A schematic cross section of a single PEMFC showing the different components and the reactions taking place.

Hydrogen gas (H_2) enters the fuel cell at the anode side and makes contact with the catalyst on the electrode surface. The hydrogen molecules break apart upon bonding to the platinum surface forming weak H-Pt bonds (Equation 2-1). Each hydrogen atom releases two electrons (e^-) (Equation 2-2 and 2-3), which travel around the external circuit to the cathode. The remaining hydrogen proton travels through the membrane material to the cathode (Equation 2-4).

At the cathode oxygen molecules (O_2) come into contact with platinum catalyst, breaking apart upon bonding to the platinum surface forming O-Pt bonds. (Equation 2-5 and 2-6). Since the protons are positively charged and the oxygen atoms are negatively charged, they

will attract each other through the proton conducting membrane and will combine to form a water molecule (H_2O) at the cathode. The overall cell reaction is shown in Equation 2-7.

The electrode reactions read:

Anode reaction
At the anode hydrogen is electrochemically oxidized to form protons and electrons.

$2Pt(s) + H_2(g) \rightarrow 2(Pt\text{-}H_{ads})$ Equation 2-1

$2(Pt\text{-}H_{ads}) \rightarrow 2H^+ + 2e^- + 2Pt(s)$ Equation 2-1

$H_2 \rightarrow 2H^+ + 2e^-$ Equation 2-2

Membrane transfer
The protons are transported through the membrane.

$H^+(an) \rightarrow H^+(cat)$ Equation 2-3

Cathode reaction
At the cathode oxygen is electrochemically reduced and combines with the hydrogen that is transported through the membrane and the electrons that pass through an external circuit. The oxygen reduction reaction is a multi electron transfer process which involves several elementary steps with corresponding generation of intermediate species. The overall mechanism of direct electrochemical reduction of O_2 to water is a direct four-electron pathway.

$Pt(s) + O_2 \rightarrow Pt\text{-}O_2$

$Pt\text{-}O_2 + H^+ + e^- \rightarrow Pt\text{-}O_2H$ Equation 2-4

$Pt\text{-}O_2H + 3H^+ + 3e^- \rightarrow Pt(s) + 2H_2O$

$½O_2 + 2H^+ + 2e^- \rightarrow H_2O$ Equation 2-5

The limiting step in the ORR is the breakage of the O-O bond. The ideal reaction (on pure Pt at low current densities) is the direct four electron reaction (as described in the above equation). When Pt is supported on carbon and at high current densities, the ORR appears to occur by several possible pathways (in aqueous solutions). Two of the possible pathways are the direct four electron reduction and a two electron “peroxide” pathway, which involves H_2O_2 as intermediate specie (see Equation 2-7). This pathway occurs due to the kinetics of the breakage of the O-O bond.

$O_2 + 2H^+ + 2e^- \rightarrow H_2O_2$ Equation 2-7

Peroxide can undergo further reduction:

$H_2O_2 + 2H^+ 2e^- \rightarrow 2H_2O$ Equation 2-8

$H_2O_2 \rightarrow 2H_2O + O_2$ Equation 2-9

Overall cell reaction

The overall reaction in the cell is the sum of Equation 2-3 and Equation 2-6 and is the electrochemical oxidation of hydrogen to form water.

$H_2(g) + ½O_2(g) \rightarrow H_2O(l)$ Equation 2-10

2.2 Electrolyte membrane

In a PEMFC a thin ion-conducting polymer membrane is utilized as the electrolyte. The membrane allows protons to pass through to the cathode side, but separates hydrogen and oxygen molecules and prevents direct combustion. The membrane also acts as an electronic insulator between the flow field plates.

The proton conducting membrane usually consists of a PTFE-based polymer backbone to which sulfonic acid groups are attached. The most common membrane material used today is Nafion®. Nafion consists of perfluorosulfonic acid polymer chains with a fluorocarbon or hydrocarbon backbone (Figure 2). The acid molecules are fixed to the polymer and cannot leak out. However, the protons on these acid groups are free to migrate through the membrane.

Ions are conducted via ionic sulfonic acid groups within the polymer structure that are dependent on water to conduct efficiently [2]. This limits the operating temperature of PEMFC to under the boiling point of water and makes water management a key issue in PEMFC development.

The conductivity of the membrane is sensitive to contaminations. If the membrane is exposed to metallic impurities, metal ions could diffuse into the membrane and displace protons as charge carriers, which would lower the membrane conductivity.

Typical thickness of a membrane is 25-50µm in a state of the art PEMFC for hydrogen-air fuel.

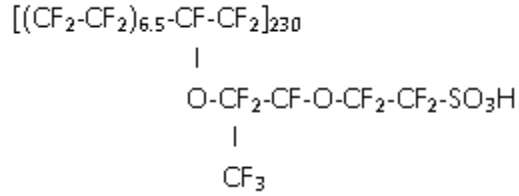

Figure 2 Perfluorosulfonic acid polymer chain

2.3 Electrodes

All the electrochemical reactions take place at the electrode surfaces. The ORR at the cathode is inefficient and limits the achievable power density and efficiency of the PEMFC.

To speed up this reaction the electrodes contains platinum. The electrodes are constructed with high surface area platinum particles dispersed on high surface area carbon supports. In addition to the porous mixture of carbon supported platinum the electrodes contains a proton conducting polymer.

The catalyst layer is porous so that a large surface area can be exposed to the oxidants and the reactants. To increase the platinum utilization the platinum catalyst should be in contact with the proton conducting polymer, the platinized carbon and the gas feed. Catalyst not in contact with all three phases will not contribute to the reaction.

The thickness of the catalyst layer in a PEMFC is typically 10µm.

2.4 Gas diffusion layer

The MEA is sandwiched between the flow field plates. On each side of the MEA, between the electrode and the flow field plate, the gas diffusion layer (GDL) is placed. The function of the GDL is to drain liquid water, transport gases (H_2 and O_2 from air) and to conduct electrons. The GDL is usually made from carbon fiber or carbon cloth and is usually treated with a fluoropolymer and carbon black to improve water management and electrical properties. Typical thickness of the GDL is between 200 and 400µm.

2.5 Flow field plates (current collectors)

The flow field plates in a single PEMFC connect the cell electrically and deliver reactants and oxidants via flow channels. The flow channel geometry has an effect on reactant flow velocities and mass transfer thus affecting fuel cell performance.

The flow field plate material must have a high conductivity and be corrosion resistant and chemically inert. Commonly used materials are solid graphite and stainless steel. Solid graphite is highly conductive, resistant to corrosion and chemically fairly resistnat. Stainless steel must often be coated to prevent corrosion and to reduce contact resistance.

As mentioned in section 2.2 the membrane is sensitive to impurities and especially to metallic impurities. The biggest source of metallic impurities comes from the flow field plates and the choice of materials would directly affect PEMFC lifetime.

2.6 Theory of operation

The basic theory of PEMFC operation is well covered [3]. This section briefly explains the different loss mechanisms and operational factors affecting PEMFC performance and lifetime. Some important equations are given in Appendix A.

2.6.1 Cell performance

The most common way to characterize a fuel cell is by obtaining a polarization curve (Figure 3). The characteristic shape of the curve is mainly a result of different irreversibilities (A, B and C in the list below). The four major irreversibilities in fuel cells are listed below.

A: Activation losses: Caused by the slowness of the reactions taking place (reaction kinetics) on the surface of the electrodes. A proportion of the voltage generated is lost driving the chemical reaction that transfers the electrons from one electrode to the other.

B: Ohmic losses: This voltage drop is the ohmic resistance to the flow of electrons through the materials of the electrodes and the various interfaces.

C: Mass transport or concentration losses: These result from the change in concentration of the reactants at the surface of the electrodes as the fuel is used. Because the reduction in concentration is the result of a failure to transport sufficient reactant to the electrode surface, this type of loss is also often called mass transport loss.

D: Fuel crossover and internal current losses: This energy loss results from the waste of fuel passing through the electrolyte. The fuel loss is usually small, and will not be considered in detail here.

Each of the above described overpotentials dominates in different current density regions. As shown in Figure 3, activation overpotential dominates at low current density (region A) (due to the activation limited oxygen reduction reaction), ohmic losses dominate in the middle region (region B) and mass transport overpotential dominates when the current density increases (region C) (This is mainly due to higher water production and the higher flow rates demanded at higher current densities).

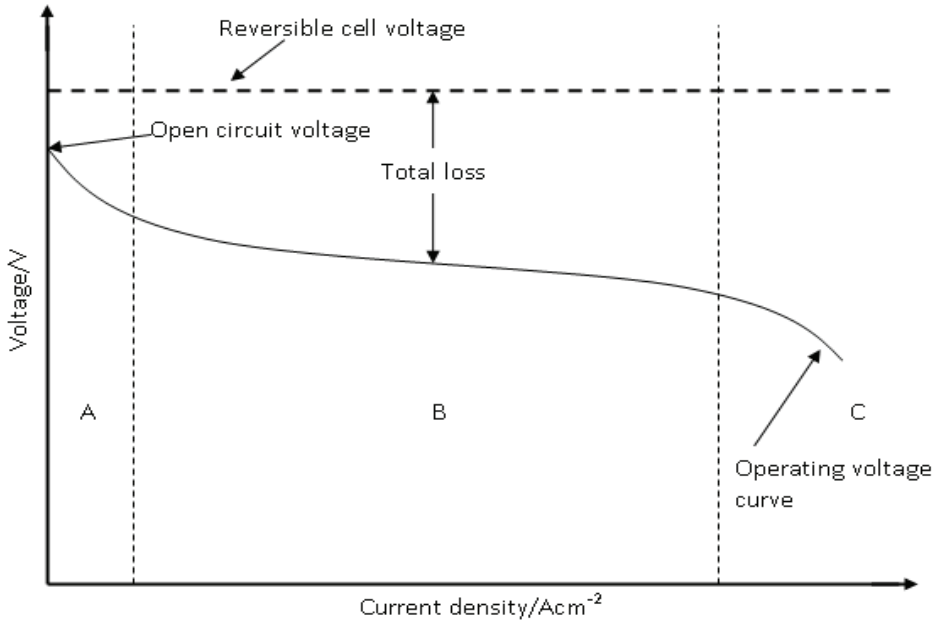

Figure 3 Typical cell potential-current-density relation for a PEMFC, with three distinct regions A, B and C.

Definitions and formulas for the OCV, the reversible cell potential and the different losses are given in Appendix A.

2.6.2 Effect of operating conditions on performance

2.6.2.1 Humidification

Accumulation, transport and formation of liquid water (see overall cell reaction Equation 2-10) are important factors in the operation and performance of the PEMFC. Water content of the MEA and the GDL has an effect on overpotentials and loss mechanisms and the cell performance could be affected negatively by both drying and flooding.

It is common to supply water through both the anode and cathode gases to humidify the materials and hence ensure good performance [4]. Water is also produced during the electrochemical reaction at the cathode. Without proper water management, liquid water may accumulate in the porous materials and block the reactant gases from reaching the catalyst sites, which results in a decrease in power density of the PEMFC. In this way the water management directly affects the power density.

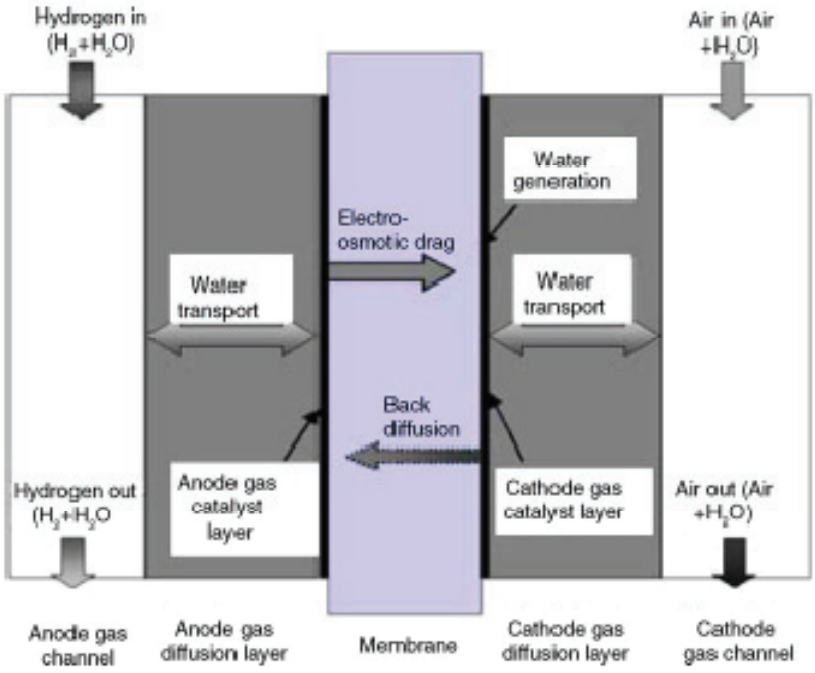

Figure 4 Schematic of the water transport process in a typical hydrogen PEMFC. [4]

Figure 4 gives an illustration of the water transport processes occurring in a PEMFC. The electro-osmotic drag is a measure of the number of water molecules that are carried with each proton travelling from the anode to the cathode. Due to hydrogen bonding, on average 1 to 2.5 water molecules are dragged along with each proton as it travels from the anode to the cathode. The osmotic-drag mainly depends on the temperature and water content in the cell. The production of water at the cathode results in a gradient in the water activity across

the membrane. This gradient will result in diffusion of water from the cathode to the anode (back diffusion).

The water management in PEMFC is a complex topic and is widely discussed in other literature [4].

2.6.2.2 Fuel cell temperature

One of the key factors when controlling the water management of a fuel cell is the temperature. The amount of water the air can contain is exponential to the temperature, and a small change in temperature will have a great influence on the hydration of the cell (See Figure 5).

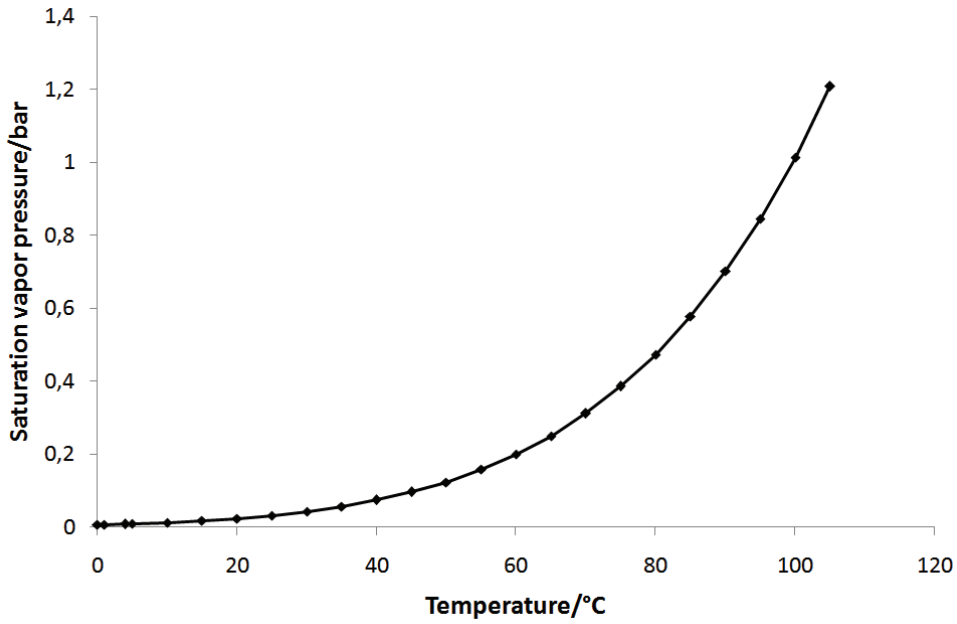

Figure 5 Saturation vapor pressure of water[1]

In addition the fuel cell temperature would affect the reaction kinetics.

2.6.2.3 Clamping pressure

In a PEMFC the contact resistance causes potential losses across the fuel cell [5]. The contact resistance could be reduced by compressing the materials (See schematic representation in Figure 6).

[1] Data from "SI Chemical Data", 4th edition, G. Aylward & T. Findlay

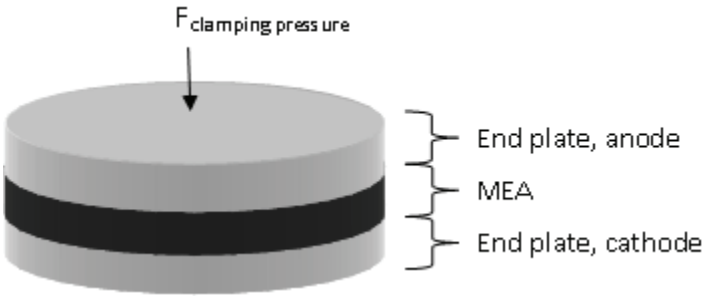

Figure 6 Schematic representation of clamping pressure where $F_{clamping\ pressure}$ represents the mechanical pressure over the MEA.

The effect of clamping pressure can be summarized to:

Low clamping pressure results in a high interfacial resistance between the catalyst layer and the GDL and between the bipolar plates and reduces the electrochemical performance of the cell.

High clamping pressure reduces the contact resistance between the GDL and the bipolar plate, but it also restricts and limits the diffusion path for mass transfer from the gas channels to the catalyst layer which could reduce the electrochemical performance.

Variation of clamping pressure results in a variation of power density. This shows that an optimal clamping pressure may exist for a given design. This optimum depends on the materials used in the fuel cell and the fuel cell design.

In addition, with variation in temperature and water content, clamping pressure could stretch the membrane leading to irreversible damage.

2.6.2.4 Back pressure

A fuel cell is typically operated at elevated pressures to ensure proper flow of reactants at the electrodes. In addition elevated pressures increase the kinetics of the electrode reactions at the cathode and increase the reversible OCV (Equation 2-11).

$$\Delta E^{rev} = \Delta E^{0} + \frac{RT}{nF} \ln\left(\frac{P_{H_2} \cdot P_{O_2}^{0.5}}{P_{H_2O}}\right) \qquad \text{Equation 2-11}$$

Another important factor when considering pressurization is the water management in the fuel cell. By increasing the pressure the volumetric flow would reduce (see Equation 2-12) and hence reducing the amount of water carried out of the fuel cell. This would especially be beneficial when running with low relative humidity (rH < 100%).

$$p\dot{V} = \bar{R}T \qquad \text{Equation 2-12}$$

2.7 Degradation

When considering PEMFC durability and lifetime the different mechanisms that degrade the fuel cell components and the conditions affecting these mechanisms must be studied. In PEMFCs the electrochemical energy conversion takes place in the MEA and the MEA is therefore more prone to chemical and electrochemical degradation.

Several factors can reduce the lifetime of a PEMFC, including platinum particle dissolution and sintering, carbon corrosion and chemical attack of the membrane. These factors are highly connected to the conditions under which the fuel cell is operated. Important operating conditions include fuel cell temperature, voltage and current, pressures and humidity.

Although research on PEMFC durability has increased in recent years, few review papers cover this area and some of the described degradation mechanisms are controversial and not fully understood. Based on available articles this chapter will summarize different aspects when considering PEMFC durability and lifetime.

2.7.1 Catalyst durability

When considering PEMFC durability the stability of platinum particles on the carbon support material are of high importance. Loss in electrocatalyst surface area is mainly due to the growth of platinum particles. Typical electrode degradation modes are:

- Corrosion of the carbon materials in the electrodes (both catalyst support and GDL materials)
- Corrosion of the catalyst material (both particle growth and dissolution, Ostwald ripening mechanism)
- Loss of proton conductivity

All these degradation modes are a strong function of the operating conditions such as temperature, reactant gas partial pressures, relative humidity, operating voltage and and overvoltages [6].

2.7.1.1 Corrosion of the catalyst support

To reduce the noble metal requirement, platinum is usually supported on carbon in the form of dispersed particles. This allows for high catalyst surface area at low catalyst loadings. However, carbon supported catalysts are receptive to catalyst particle agglomeration and are thermodynamically unstable at typical operating conditions of the air electrode in PEMFCs.

Both the anode and cathode of PEMFC operates at low pH (<1), relative high temperature (~80°C) and with high levels of water both in vapor and liquid phase, an environment where the carbon supported catalyst could oxidize to carbon dioxide. Oxidation of carbon support is generally referred to as carbon corrosion and could lead to performance losses due to loss of active surface area and change in surface characteristics [7].

The equilibrium potential for carbon oxidation to carbon dioxide is 0.207 V relative to a Reversible Hydrogen Electrode (RHE) at 25°C.[2] This means that the electrochemical oxidation of carbon is thermodynamically possible above 0.2V. However, due to carbon kinetics the voltage needed for oxidation of carbon typically above 1 V. Equation 2.13 – Equation 2-15 describes different pathways for carbon oxidation..

$C + 2H_2O \rightarrow CO_2 + 4H^+ + 4e^-$ $E_{oo} = 0.207$ V Equation 2-13

$C + H_2O \rightarrow CO + 2H^+ + 2e^-$ $E_{oo} = 0.518$ V Equation 2-14

$CO + H_2O \rightarrow CO_2 + 2H^+ + 2e^-$ $E_{oo} = -0.103$ V Equation 2-15

CO formed from CO_2 reduction could desorb from the surface, enter the gas flow and re-adsorb further down the gas channel. The reduction of CO_2 needs the presence of hydrogen atoms adsorbed on the catalyst surface (see Equation 2-16).

$CO_2 + 2Pt\text{-}H \rightarrow Pt\text{-}CO + H_2O + Pt$ Equation 2-16

The oxidation of carbon would decrease the amount of carbon available for Pt loading, which forces Pt particles to detach from the carbon support and decreases the electrochemical surface area (see schematic representation in Figure 7).

Under operation the fuel cell will experience different conditions between the inlet and outlet, which can lead to an uneven reactant distribution. In the case of complete fuel starvation, cell voltage can become negative as the anode is elevated to positive potentials and the carbon is consumed instead of the absent fuel. In the absence of a sufficient anodic current source from hydrogen, the cell potential climbs higher until oxidation of the carbon support of the catalyst layer occurs. This situation would lead to carbon corrosion to form carbon dioxide and result in permanent damage to the anode catalyst layer.

Local fuel starvation can induce local potentials on the air electrode higher than 1V and, thereby, induce corrosion of the carbon supports. The problem with local fuel starvation under normal operation can be reduced with careful control of reactants and water management. However, under start up and shot down localized fuel starvation is almost certain to exist.

The problem with fuel starvation can be induced not only by poor cell-to-cell flow distributions but also by local blockage, by water blockage and by differences in channel depth tolerance.

High temperature and humidification levels increase carbon corrosion significantly [8].

2.7.1.2 Catalyst corrosion

The size of the Pt-based catalyst used in PEMFC is usually in the range of 2-6 nm. Smaller particles sizes results in a higher specific surface area. However, these nanoparticles tend to

[2] Data from ”SI Chemical Data”, 4th edition, G. Aylward & T. Findlay

agglomerate due to their high specific surface energy [9]. When Pt particles agglomerate the electrochemical surface area of Pt catalyst decreases [9].

Operating PEMFC at high cell voltage would result in an increase of the cathode electrode potential, under which surface oxides of Pt are formed [6]. This would again decrease the Pt activity toward ORR and accelerate the degradation of Pt catalyst [6]. Compared to operation with high cell voltage the corrosion of catalyst is higher under open circuit situations [10].

In the case of fuel starvation hydrogen is no longer available to be oxidized and the anode potential will rise to a level where water will oxidize, which again could produce oxidative species or the carbon support at the anode could oxidize [11]. In the same way as described for the catalyst support the catalyst layer could corrode when exposed to local fuel starvation.

It is shown that under typical fuel cell operating conditions the platinum particles tends to go through a ripening process (Ostwald ripening) that is most pronounced during the first 500 hours of operation of the fuel cell [12]. This ripening process can either be a dissolution process or a crystallite surface diffusion and growth mechanism. The surface diffusion can either be crystals that dissociate and metal atoms that diffuse on the surface to associate with bigger particles, or it could be migration of crystallite that collide and coalesce on the support surface (See Figure 7).

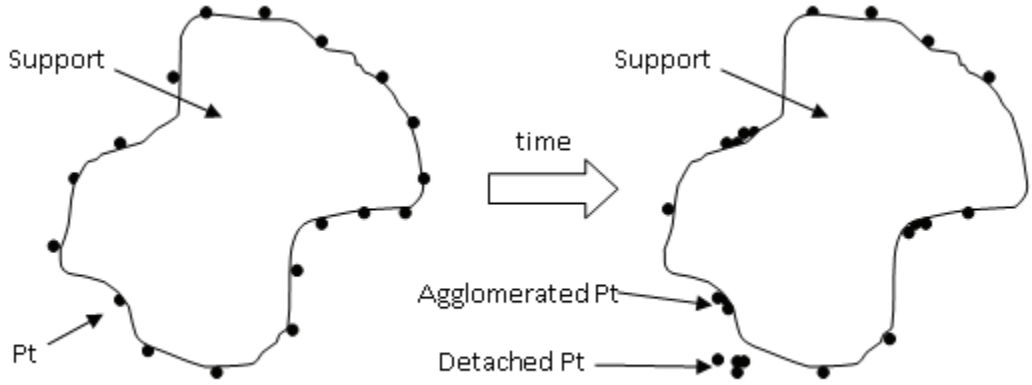

Figure 7 Schematic representation of Pt agglomeration and Pt detachment from catalyst support surface [9].

Humidification levels and fuel cell temperature could affect the lifetime of the MEA. Knights et al. [13] compared different humidity levels and found large differences in the observed lifetime of the MEA. When the humidification at the anode was kept at 100% RH and 70% RH at the cathode the MEA lifetime was longer (~3250 hours) than when the humidification was kept at 0% anode and 0% cathode (~250 hours). This difference could be explained by the difference in the rate of Pt-band formation, which again is explained by that the dissolution of Pt is greater under low humidification.

In addition the presence of liquid water could increase the growth rate of Pt particles. It is suggested that the water penetrates between the particles and the support and lower the bonding energy [14].

Investigation of potential cycling of Pt electrodes has shown that Pt dissolves and that the Pt surface area changes with time with potential cycling [15]. In a potential cycle the cathode experience potential variations as the cell potential changes to mach variable power demands. The variation of the cathode potential will change several properties of the electrode materials, including the degree of oxide coverage of both platinum and carbon and the hydrophobicity of the surfaces.

2.7.2 Membrane degradation mechanism

Membrane degradation can take place as both physical thinning and as loss in ionic conductivity of the membrane. Both cases affect the fuel cell performance negatively. It is usual to divide membrane degradation into chemical and mechanical degradation.

2.7.2.1 Chemical degradation

The membrane in PEMFC is subjected to both a chemically oxidizing environment on the cathode and a chemically reducing environment on the anode. In addition, radicals formed in the fuel cell could attack the membrane. Chemical degradation of PEM membranes is mainly attributed to these attacks.

Several mechanisms are proposed for the formation of peroxides and radicals. Some of them are addressed below.

One of the possible mechanisms for chemical degradation of the membrane is oxidation of the membrane material. One of the species that will oxidize the membrane is hydrogen peroxide (H_2O_2). Liu [16] has been able to observe the existence of hydrogen peroxide in an in-situ PEMFC test. It is shown that the concentration of hydrogen peroxide is primarily depended on membrane thickness where thinner membranes display higher peroxide concentrations. Liu also concluded that peroxide is most likely formed on the anode side of the cell through reduction of O_2. Results from Mittal [17] supports this statement.

As mentioned in section 2.1 hydrogen peroxide could be produced as an intermediate product in the ORR. A typical scheme representing the overall ORR for acidic conditions is shown in Figure 8 [18].

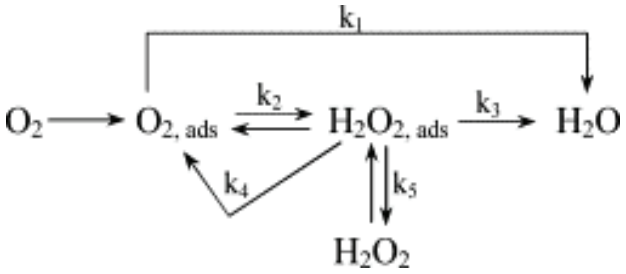

Figure 8 Overall oxygen reduction reaction for acidic conditions [18].

In addition to the incomplete reduction of oxygen at the fuel cell cathode the formation of peroxide radical could also be generated at open circuit conditions with interaction of hydrogen and crossover oxygen at the anode.

Hydrogen peroxide (H_2O_2) is also formed when oxygen molecules permeate through the membrane from the cathode side and are reduced at the anode Pt catalyst (See Equation 2-17 – Equation 2-19) [19]. The formation of H_2O_2 can occur at a higher rate when high stoichiometry of reactants is present because of a greater excess of reactants available for peroxide formation.

$H_2 + Pt \rightarrow Pt\text{-}H$ (at anode) Equation 2-17

$Pt\text{-}H + O_2$ (diffused through PEM to anode) $\rightarrow {}^{\bullet}OOH$ Equation 2-18

${}^{\bullet}OOH + Pt\text{-}H \rightarrow H_2O_2$ Equation 2-19

Then at the anode the H_2O_2 diffuses into the membrane and reacts with bivalent metal cations (M^{2+}), present as impurities in the membrane to form active oxygen species, which then attack the polymer and degrade the membrane.

$M^{2+} + H_2O_2 \rightarrow M^{3+} + {}^{\bullet}OH + OH^-$ Equation 2-20

$M^{3+} + H_2O_2 \rightarrow M^{2+} + {}^{\bullet}OOH + OH^+$ Equation 2-21

Hydroxy (${}^{\bullet}OH$) and hydroperoxy (${}^{\bullet}OOH$) radicals are some of the most reactive chemical species known in fuel cells and are the most likely initiators of chemical degradation of the membrane. Theses radicals attack the membrane and could lead to cleavage of the perfluorocarbon backbone in PFSA membranes. This affects the proton conductivity and the mechanical strength of the membrane.

One assumption made about degradation of perfluorosulfonated membrane is that it starts at the unstable polymer end-groups, such as –COOH, -COF and $-CF_2H$ [20]. First they oxidize to carboxyl groups and then the carboxyl groups undergo the degradation via unstable – CF_2OH and –COF with the release of HF [20]. After a cycle of this degeneration process, carboxyl groups are regenerated and subjected to further degradation (unzipping reaction at unstable polymer end-groups).

Hommura et al. [20] concluded that membrane degradation reactions are composed of not only the unzipping reaction at unstable polymer end-groups but also of a scission mechanism of main chains to form carboxyl groups at severed points (see illustration in Figure 9).

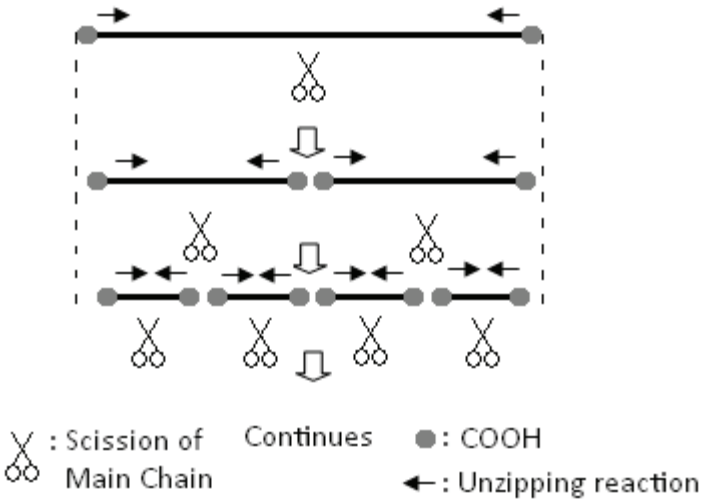

Figure 9 Degradation mechanism of perfluorosulfonated membrane [20].

Excess water could result in reactant diffusion blockages, particularly on the cathode, causing an increase in mass transport losses. Another effect is that the presence of excess water could negatively affect cell performance by transporting impurities within the cell and depositing them on the catalyst or the membrane where they modify electrode performance and the electrolyte ionic conduction mechanism leading to increased ohmic and mass transport loss. Even in the absence of impurities, prolonged exposure of the MEA to excess water may also result in a permanent loss of performance attributed to material degradation such as reduction in hydrophobicity [21].

It is reported that membrane degradation is accelerated under low humidity conditions [22]. The OCV under low humidity conditions rapidly decline compared to that under high humidity conditions.

2.7.2.2 Mechanical degradation

Mechanical degradation occurs in many forms including cracks, tears, punctures or pinhole blisters and is often the cause of early life failures. Baldwin et al. [23] stated that mechanical failures is the main cause of membrane degradation rate.

During operation of PEMFCs, the MEA is put under compressive force between the bipolar plates. This compressive force can with time deform the MEA and cause permanent thinning and eventually failure in form of pinholes or cracks. In combination with chemical degradation and other physical degradation routes, deformation can be an important factor in MEA degradation. In addition a non uniform pressure between the MEA and the bipolar plates during fuel cell operation can result in local compressive stresses and will accelerate membrane degradation.

It is suggested that physical thinning of the MEA is accelerated under inadequate water content due to low humidification of the feed stream [24]. Tang Y. et al. [25] have experimentally investigated the effects of humidity and temperature on the mechanical properties of perfluorosulfonic acid membranes. Results indicate that stresses decrease as humidity and temperature increase and that lack of water makes the membrane brittle and

fragile. Changes in temperature and relative humidity during cycling can cause stresses in the membrane which can generate and propagate small tears in the membrane.

In addition reduced water for heat transfer removal could result in increased local temperatures, which again could result in membrane failure. Dry membrane conditions could also result in loss in proton conductivity [21].

Large particles in the catalyst layer or fibers from the carbon fiber paper can slowly creep through the membrane leading to electrical shorting and membrane pinhole failure. It is suggested that in the membrane cracks are initiated at catalyst defects and by the penetration mechanism [24].

In the membrane pinholes and cracks would lead to increased crossover which again would lead to increased catalyst degradation.

2.7.3 Degradation of the gas diffusion layer

Like the membrane and the electrocatalyst the GDL of a fuel cell can undergo degradation which would alter the transport properties for gases and water. Usually the GDL is impregnated with a hydrophobic material to make it water repellent. It has been shown that the GDL loses its hydrophobicity with time [24].

The PEMFC operating environment gradually changes the GDL from hydrophobic to hydrophilic, which can degrade fuel cell performance. Maintaining the hydrophobic character of the GDL is important to maintaining mass transport in the fuel cell since liquid water saturates the catalyst ionomer phase in the catalyst layer, restricting gas flow to the active platinum sites in the layer.

2.7.4 Impact of contaminants

One of the challenges of PEMFC systems is the low tolerance to impurities. Impurities can affect both performance and lifetime negatively. Impurities can come from the fuel and oxidant feed or released from material used in the fuel cell system. Some of the sources of impurities and their origin are shown in Table 1.

Impurity source	Typical contaminant
Air	NO_x, SO_x, NH_3, O_3
DI water	Si, Al, S, K, Fe, Cu, Cl, Cr, formic acid
Bipolar plates	Fe^{3+}, Ni^{2+}, Cu^{2+}, Cr^{3+}
Membranes	Na^{+}, Ca^{2+}

Table 1 Contaminants identified in the operation of fuel cells.

Impurities that adsorb onto the anode or cathode catalyst surface affect the electrode charge transfer processes, resulting in overpotential losses. Cations produced or introduced to the cell can cause ion exchange with protons in the ionomer. These cations would lower

the proton conduction and could result in increased ohmic losses. Performance losses due to impurities can be permanent, or reversible.

Pozio et al. [23] have investigated the effect of cations released from different metals used as end plates on the lifetime of the membrane. The end plates were not in direct contact with the electrodes. Ions that are strongly bonded to the sulfonic groups of the membrane will block the proton transport through the membrane. The experiment found that the membrane suffered from severe fluoride losses. This mechanism could be explained with the classical Fenton's reaction mechanism (Equation 2-22 and 2-23).

$$M^{2+} + H_2O_2 \rightarrow M^{3+} + OH^{\bullet} + OH^{-} \qquad \text{Equation 2-22}$$

$$M^{3+} + H_2O_2 \rightarrow M^{2+} + OOH^{\bullet} + OH^{+} \qquad \text{Equation 2-23}$$

However, there exist different views on this mechanism and several modifications of the classical Fenton's reaction mechanism are suggested.

For a more detailed description on impurities and their impact on PEMFC lifetime and performance see Cheng et al. [26]. Cheng et al. have reviewed over 150 articles on the subject of the effect of contaminations on PEMFC. This review focuses on contamination impacts on PEMFC performance, mechanism approaches and mitigation development.

2.7.5 Summary of MEA degradation

- MEA degradation must be understood from both chemical and mechanical perspectives.
- Higher temperature accelerates chemical degradation.
- Lower relative humidity accelerates degradation.
- Crossover reactant gases that reacts with Pt lead to peroxyl species (H_2O_2, $HO^{\bullet}$, $HOO^{\bullet}$) generation that chemically degrades the membrane.
- Mechanical degradation occurs in many forms including:
    - Tear initiation and propagation
    - Cracks initiated by catalyst defects
    - Particle penetration
- Cycling and low relative humidity could promote mechanical degradation modes.
- Contaminants will accelerate chemical degradation.

3 Durability testing methods

There exist various methods for measuring PEMFC degradation. It is common to categorize by *in-situ* and *post mortem* methods. The most common post mortem methods are TEM and SEM measurements. To be able to collect time dependent information from these tests several cells must be run in parallel under the same conditions and at different times. *In-situ* methods have the advantage that they can give instant information during the operation of a PEMFC. This section will focus on *in-situ* methods.

3.1 Polarization measurements

The most common way to characterize fuel cells is the polarization curve. The polarization curve can give information about activation losses, ohmic losses and mass transport losses. By obtaining polarization curves at different stages during a long term degradation experiment, information about the time dependencies of the different losses can be evaluated. However, polarization curves must be used in combination with other methods to break the losses down into their contributing parts.

3.2 Cyclic voltammetry

The electrochemical active area of the platinum catalyst is commonly measured with cyclic voltammetry (CV). CV is a potential controlled electrochemical experiment where a potential sweep is imposed on an electrode and the faradaic current response is measured (a faradaic current is the current due to a redox reaction). This current response can give information about the adsorption and desorption of hydrogen. Results from a CV scan can then be used to calculate the active area for the cell.

The applied potential is varied from an initial value in a linear manner up to a pre defined limiting value (apex). At this potential the direction of the potential scan is reversed and the potential window is scanned in the opposite direction. By doing this the species formed by oxidation on the forward scan can be reduced on the reversed scan. In addition to providing an estimate of the redox stability the scan provides information about the rate of electron transfer between the electrode and the analyte.

A common setup for cyclic voltammetry is shown in Figure 10 and contains three electrodes: the working electrode (WE), counter electrode (CE) and the reference electrode (RE).

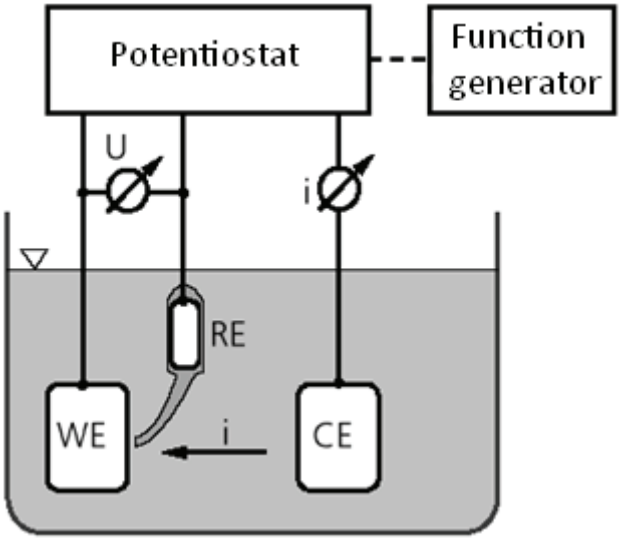

Figure 10 Experimental setup for cyclic voltammetry [27].

The electrode under investigation is the working electrode. The reference electrode is used to measure the working electrode potential. On the counter electrode a reversible reaction takes place. This reaction provides conservation of charge. The potential at the working electrode is swept several times between the minimum and maximum potential. Figure 11 shows an example of a CV curve (current (i) vs. voltage (U)) from one cyclic sweep on polycrystalline Pt in an acid environment.

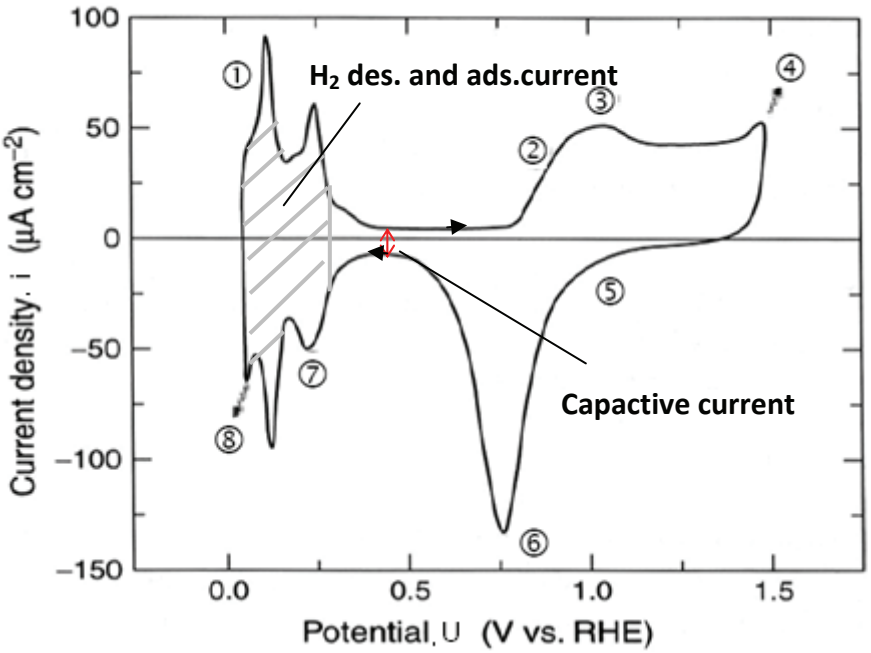

Figure 11 Example of a CV curve on polycrystalline Pt in an acid environment [27].

The characteristic shape of the curve is a result of different processes taking place at the working electrode surface. Related to Figure 11 the following reactions take place.

Step	Descritption	Reaction
1	H_2-desorption	$Pt\text{-}H + H_2O \rightarrow Pt + H_3O^+ + e^-$
2	O_2-adsorption	$Pt + 2H_2O \rightarrow Pt\text{-}OH + H_3O^+ + e^-$
3		$Pt\text{-}OH + H_2O \rightarrow Pt\text{-}O + H_3O^+ + e$
4	O_2-development	$Pt + 2H_2O \rightarrow Pt\text{-}OH + H_3O^+ + e^-$
		$Pt\text{-}OH + H_2O \rightarrow Pt\text{-}O + H_3O^+ + e$
		$2Pt\text{-}O \rightarrow 2Pt + O_{2,g}$
5	O_2-desorption	$Pt\text{-}O + H_3O^+ + e \rightarrow Pt\text{-}OH + H_2O$
6		$Pt\text{-}OH + H_3O^+ + e^- \rightarrow Pt + 2H_2O$
7	H_2-adsorption	$Pt + H_3O^+ + e^- \rightarrow Pt\text{-}H + H_2O$
8	H_2-development	$Pt + H_3O^+ + e^- \rightarrow Pt\text{-}H + H_2O$
		$2Pt\text{-}H \rightarrow 2Pt + H_{2,g}$

Table 2 Reactions taking place at the working electrode during a CV scan [27].

To do a similar experiment in a fuel cell with two electrodes, the reference and counter electrode is clamped together. Hydrogen is flushed in to the electrode chamber and due to the low overpotential the potential could be seen as constant. Since the hydrogen reaction is reversible the electrode could be used as the counter electrode at both cathodic and anodic sweep.

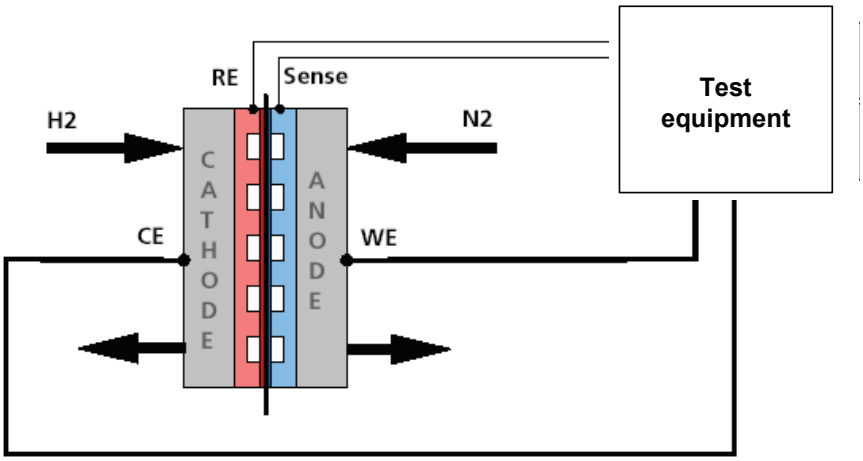

Figure 12 Setup for a fuel cell with anode as the working electrode [27].

The active area could then be calculated by taking the average from the total charge at the adsorption and desorption processes for hydrogen.

3.3 Impedance spectroscopy

One of the most common tools in the characterization of fuel cells is electrical impedance spectroscopy (EIS). This method is especially useful in systems where the performance is governed by a number of coupled processes proceeding at different rates.

In a simplified model fuel cells can be modeled with electric components as shown in Figure 13. A parallel connection of an ohmic resistance and a capacitance depicts the electrode and a pure ohmic resistance connected in series depicts the membrane.

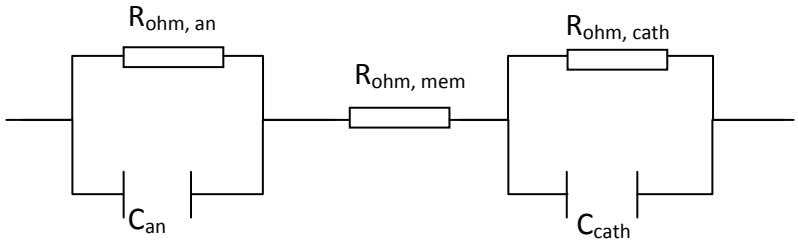

Figure 13 Equivalent electric circuit describing a fuel cell.

The capacitance can be attributed to the double-layer capacitance across the interface, while the ohmic resistance can represent the charge transfer resistance of a reaction.

The fuel cell operates under normal operating conditions (flow of hydrogen and air are set corresponding to the flow at a specified load). A small sinusoidal potential or current is applied to an electrode. The frequency of this signal is then varied over a range of frequencies and the AC (alternating current) responses of the electrodes are recorded. The wide range of frequencies employed gives an impedance spectrum which includes a range of electrode processes.

Since the rates of electrochemical reactions steps have an exponential relationship whit the electrode potential, it would be convenient to keep the sinusoidal perturbation small so the system can be assumed to be linear.

The sinusoidal current sent through the cell would conduce to charge the double-layer and to oxidize or reduce species at the electrode.

Impedance denotes a resistance to the flow of electrons or current. It can be expressed as a complex number including the real component (Z_{re}, resistance) and the imaginary component (Z_{im}, capacitance and inductance). One of the ways to present the results from an impedance spectroscopy measurement is the Nyquist plot. In a Nyquist plot the impedance is plotted vs. the real part of the complex impedance plane (See Figure 14).

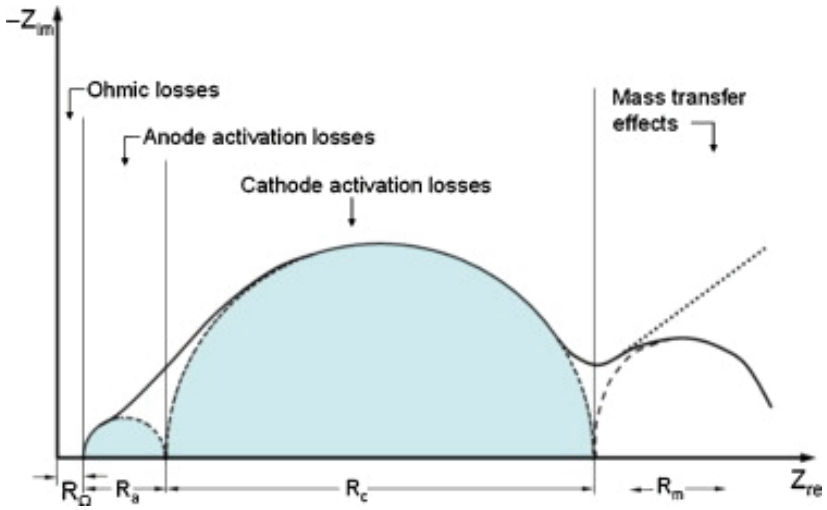

Figure 14 Nyquist plot from a hypothetical PEMFC. The four regions represent four losses in the fuel cell, and the size of each loop is correlated to the relative magnitude of each losses [28].

3.4 Hydrogen crossover

Hydrogen crossover rate is an important parameter for determination of the permeability of the membrane in fuel cells. An increase in hydrogen crossover rate from the anode to the cathode is usually explained by macroscopic pinholes formed in the membrane. When measuring the hydrogen crossover rate, the cathode gas flow is switched from air to nitrogen. The measured current corresponds to the oxidation of the hydrogen molecules at the cathode side in the presence of platinum catalyst. The anode is taken as the counter electrode, whereas the cathode serves as the working electrode.

3.5 Ohmic resistance

Ohmic losses may be measured separately by using the current interrupt technique. When a constant current load on a fuel cell system is suddenly interrupted, the voltage response with time will be representative of the capacitance and the resistance of each component. Figure 15 shows an illustration of the response of a system under a current interrupt test. In a short time scale the small capacitance associated with the double layer can be observed, which identifies activation losses ($V_{activation}$ in Figure 15). The IR drop (voltage drop due to ohmic resistance) can also be observed (V_{ohmic} in Figure 15).

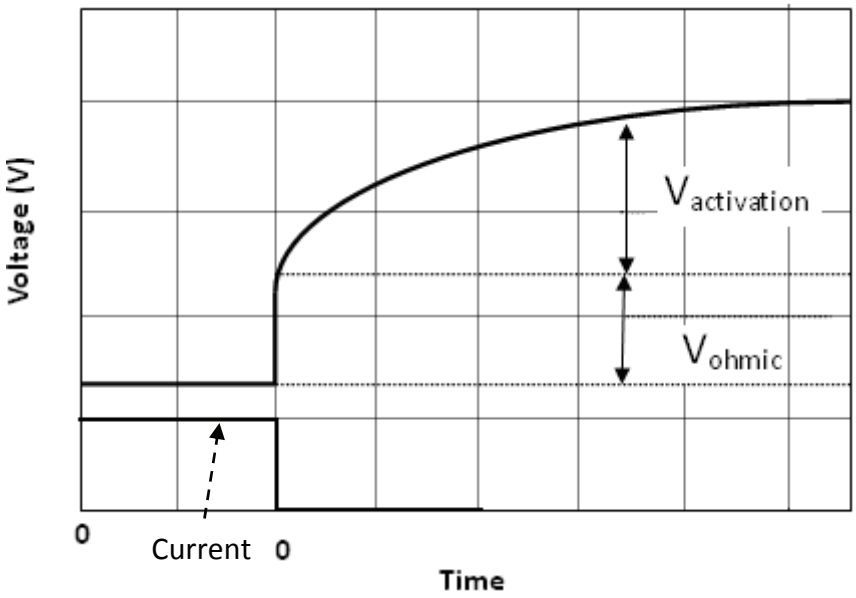

Figure 15 Illustration of a current interrupt response (current is interrupted at t0).

The charged double layer will take some time to disperse and can be seen as the curved shape in Figure 15. Compared to the activation overpotential the ohmic losses will immediately reduce to zero when the external circuit is disconnected and the current falls to zero.

3.6 Effluent analysis

A result of chemical degradation is the release of fluoride ions. The degree of chemical degradation could therefore be examined by evaluation of the fluoride ion concentration in the outlet water. It is common to use an ion chromatograph to measure the ion concentrations.

3.7 Accelerating degradation

There are several methods for accelerating PEM degradation and standard durability evaluation protocols are established. These protocols include an accelerated test methodology based on potential cycling of electrocatalyst and a protocol to measure the corrosion of catalyst support materials. The U.S. DOE and Freedom CAR Fuel Cell Technical Team have established a set of durability test protocols [29], which includes:

- Electrocatalyst cycle and metrics
- Electrocatalyst support cycle and metrics
- MEA chemical stability and metrics
- Membrane mechanical cycle and metrics

The U.S. DOE and Freedom CAR Fuel Cell Technical Team durability test protocol is attached in Appendix D.

4 Methodology

4.1 Durability test design

Degradation of PEMFC is a direct consequence of operating conditions. Durability tests have indeed reflected the combined impact from various sources (impurities, operating conditions, load cycles, etc.) on the lifetime of the MEA. However, further understanding of how the MEA degrade and the contribution and interaction of the chosen operating conditions is much needed. In addition few publications have investigated the effect of clamping pressure on PEMFC durability.

Since the goal of this thesis is to study the effect of operating conditions on PEMFC lifetime and performance and not the durability of the fuel cell components themselves, a certain level of degradation is sufficient.

In automotive applications the fuel cell will be exposed to cycles of temperature, humidities and voltages. To assess the performance and durability of fuel cell components intended for automotive applications a test protocol should be based on cycling that reflects these changes.

The design approach used in this thesis is what is called an ageing on/off test cycle. On/off cycling will promote both chemical and mechanical degradation of the MEA. The load during "on phase" is set to a relatively high level (0.8 A cm^{-2}) to accelerate the MEA degradation. Running the cell on OCV during the "off" phase will promote a uniform chemical thinning of the membrane. Switching between on and off will promote both chemical and mechanical degradation of the MEA. Recommended durability protocols from DOE (see Appendix C) and SINTEF Material and Chemistry are used to design the test protocol used in this thesis. The test procedure used is described in detail in Chapter 6.

The test duration is fixed and the screening experiment is set up as a fractional factorial design. The screening experiment is set up based on the chosen operating conditions; clamping pressure, gas humidification and back pressure.

4.2 Performance and durability assessment

The most common way to characterize fuel cells is by obtaining polarization curves. Polarization curves are therefore taken at different stages during the accelerated tests. The polarization curves will be used to evaluate degradation and to compare tests with different operating conditions.

Fluoride release is a result of local chemical or thermal degradation. Effluent water is sampled and analyzed for fluoride and sulfur periodically.

5 Experimental setup and test facilities

This chapter describes the equipment used for the experimental tests carried out in this thesis.

All the testing was carried out at SINTEF Material and Chemistry and NTNU Department of Materials Technology's fuel cell laboratories in Trondheim, Norway.

5.1 Test-station description

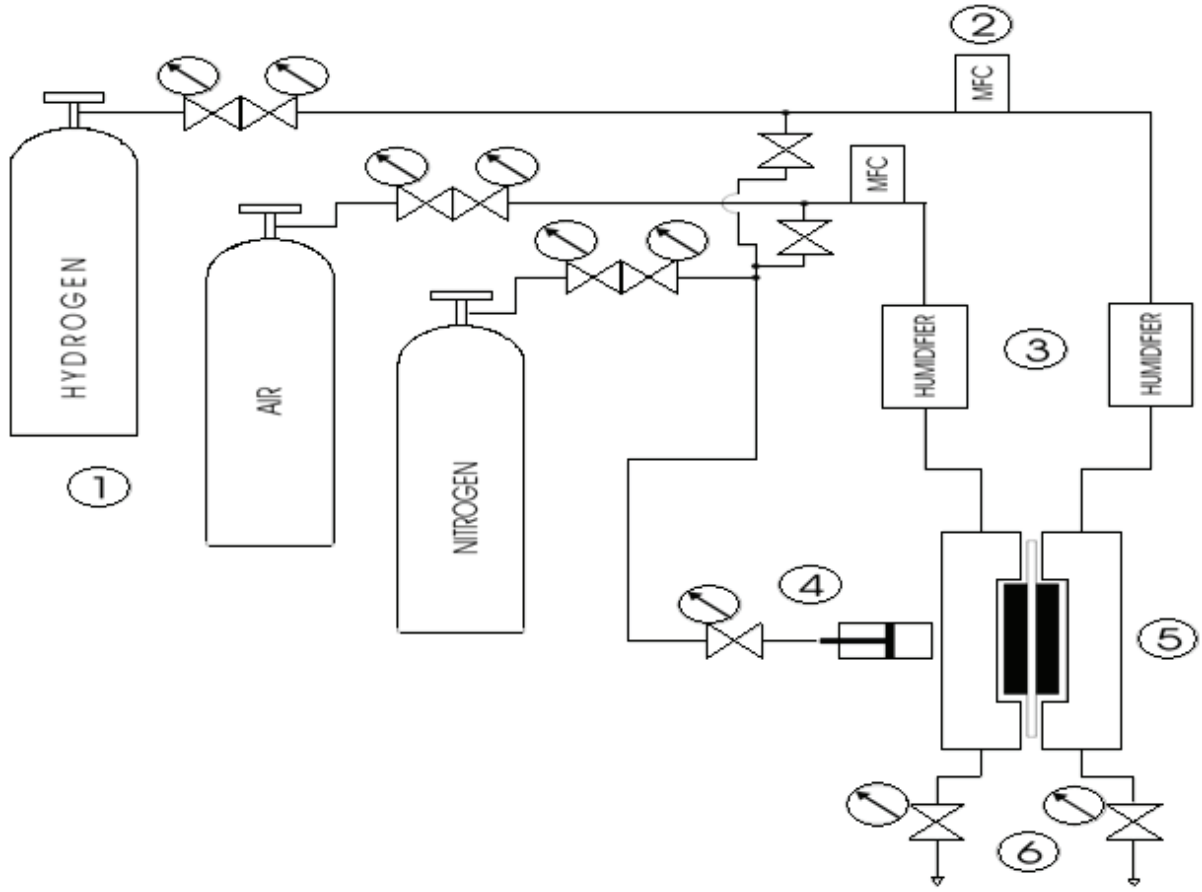

Figure 16 Flow scheme for the fuel cell test station. 1: Pressurized gas storage, 2: Electronic mass flow controllers (MFC), 3: Nafion-tube type humidifiers, 4: Pneumatic actuator for adjustment of cell clamping pressure, 5: Fuel cell under test, 6: Manual back pressure regulators [30].

The cathode is supplied with air from a pressurized container (79%N_2, 21%O_2). The anode was supplied with pure hydrogen. Flow rates were set by calibrated electronic mass flow controllers. Anode and cathode gases were humidified with a humidification system from Fuel Cell Technologies Inc.

The fuel cell temperature was set with heating elements from Watlow connected to the workstation. To control and read the fuel cell temperature type-K thermocouples were used.

Measurements were performed using LabWiew from National Instruments. Current and voltage were set using a potentiostat.

Pressure regulators from FCT are used to set the back pressures. Pressure sensors from Kobold are used to measure the gas pressures.

5.2 Clamping pressure equipment

The concept of using a pneumatic cylinder to ensure stable and reproducible clamping pressure over the MEA of the fuel cell was developed at NTNU in 1992-93 [31]. To set the pressure a pressurized nitrogen bottle is used. A pneumatic pressure system from Rexroth Mecman is used to set clamping pressures (Figure 16 nr. 4).

5.3 Test cell

The fuel cell housing used is developed at SINTEF Material and Chemistry.

A 10 cm^2 circular housing with double serpentine flow fields of stainless steel was used in a co-flow configuration. The depth of the serpentine flow field is 0.55mm.

Platinum wires measure the local cell voltage at the backing. Thermocouples measure the temperature at the outlet and inlet for both the cathode and anode gas channels (see Figure 17). Silicon gaskets are inserted around the active area to keep the cell gas-tight.

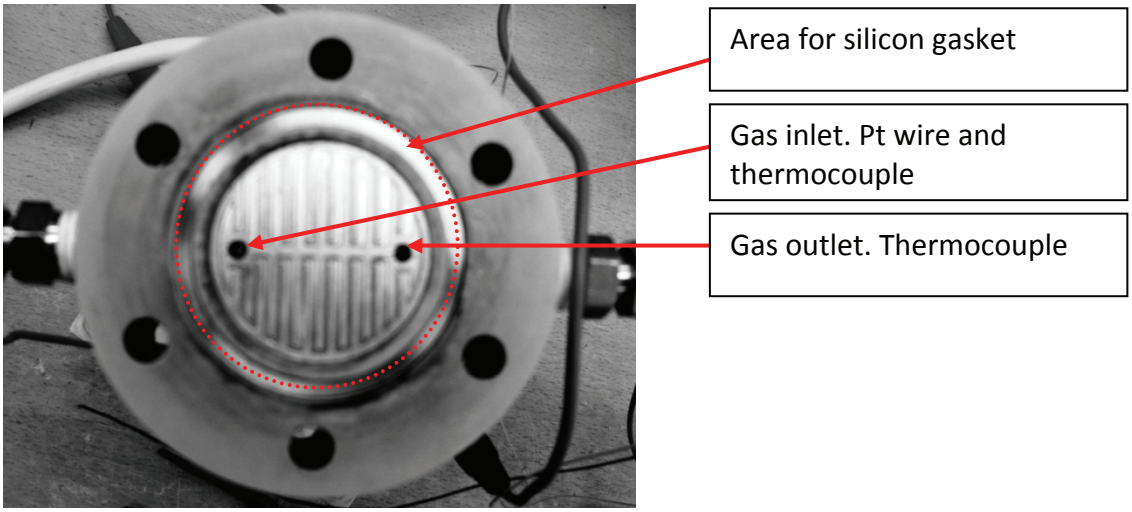

Figure 17 Picture of one side of the fuel cell housing. Arrows indicates were the platinum wire and thermocouples are inserted to measure cell voltage and temperature, respectively.

5.4 Statistical research planning

The complexity of the correlation between different factors requires a systematic approach. The experiments performed in this thesis are based on a two-level factorial design:

- Requires relatively few runs per factor studied
- Relatively simple interpretation
- Determines the direction for further experimentation
- Indication of important factors

For more information about factorial design, se Box et al.[32].

5.4.1 A 2^{3-1} experiment

Due to the large number of factors affecting PEMFC degradation it is advantageous to use statistical methods to identify the effect of the factors and their correlation.

It is evident that relative humidity will affect PEMFC performance and durability, and is therefore chosen as the first factor. Further, it is expected that back pressure will influence the cells performance and durability, and is chosen as the second factor. In earlier work it has been shown that clamping pressure has an effect on PEMFC performance [33]. However, there is little documented on the effect of clamping pressure on PEMFC durability. Clamping pressure is therefore chosen as a third factor.

To find the correlation between lifetime and performance a factorial design will be used. A full factorial design with 2 levels and 3 factors would result in 2^3 = 8 experiments. Considering the time available and the time needed to get significant degradation, it is not possible to complete a full factorial design. However, by doing a fractional factorial design (2^{3-1} = 4 experiments) it will be possible to estimate the main effects and the correlation between the three factors. The statistical design that will be used in this work is shown in Figure 18.

The factorial levels are summarized below.

Factors:

A. Relative humidity
B. Clamping pressure
C. Back pressure

Levels:

- High (+)
- Low (-)

Response: Performance (polarization measurements) and durability (mVh^{-1}).

A 2^{3-1}-fractional factorial experiment with a center level:

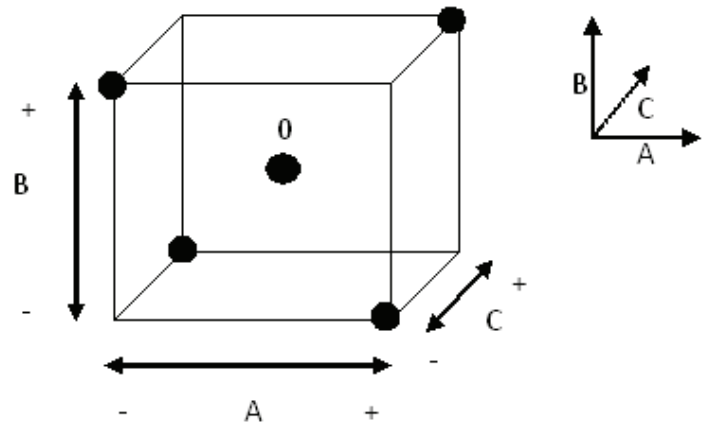

Figure 18 2^{3-1} fractional factorial design with a center-level indicated (0).

Formulation	A (A)	B (B)	C (A*B)	Response performace	Responce durability
1	-	-	+	Y_1	Z_1
2	-	+	-	Y_2	Z_2
3	+	-	-	Y_3	Z_3
4	+	+	+	Y_4	Z_4

Table 3 A 2^{3-1}-fractional factorial design.

To estimate the between-cell variance of experiments caused by cell assembly, replicates were performed.

5.4.2 Defining the operating variable space

In order to choose the variable space for the experiment, some introductory experiments were performed. All tests were performed using the same single cell with the same materials.

The initial levels for each factor are set as a compromise between what is seen as high levels and according to normal operating conditions.

The intention for the introductory tests is to see how the fuel cell and the chosen materials respond on the operating conditions.

Cell temperature was kept constant at 70°C and the humidification temperatures of the reactant gases, back pressure and clamping pressure were varied.

Appendix B shows a selection of the introductory tests where Figure 34 and Figure 35 reveals problems with the high level for clamping pressure (20 barg). Visual examination of the MEA also reveals that the high clamping pressure has torn the membrane. The high level for clamping pressure was therefore lowered.

The following variable space will be used for the durability tests:

Factors\level	High(+)	Centre (0)	Low(-)
A: Relative humidity (%)	100	50	25
B: Clamping pressure (barg)	10	7.5	5
C: Back pressure (barg)	1.5	0.75	0

Table 4 The chosen variable space.

6 Test procedure

6.1 Introduction

There exist several procedures for qualifying the generic performance of a PEMFC single cell submitted to an accelerated ageing test. The objective for these procedures is to determine the change in performance of a PEMFC single cell operating at specified conditions.

For this experiment an accelerated ageing on/off cycle test was used. The procedure used in this thesis is shown in Figure 19.

This chapter contains a description of the test procedure used in this thesis.

6.2 Pre-conditioning of test cell

To achieve maximum MEA performance and lifetime for the single cell Gore's recommended start-up procedure for PRIMEA® series MEAs (for H_2-air operation) was used. This procedure initially applied various load chemes at 100 % relative humidity and cell temperature of 70°C, and was applied until no change in performance was observed.

6.3 Setting the test conditions

After pre-conditioning the operating conditions for the actual test was set and was run until no change in performance is observed.

6.4 Ageing on/off cycling

To determine the change in OCV and the voltage on load in terms of voltage per hour the cell was submitted to a specific load profile including "on" and "off" phases of 15 minutes respectively.

The cycle follows the following profile:

- "off" phase = 15 minutes at 0 A cm^{-2}
- "on" phase = 15 minutes at i_{load} A cm^{-2}, i_{load} = 0.8 A cm^{-2}

In order to avoid important voltage drop the current density is increased step by step from 0 to i_{load} in four steps of 10 seconds (up to 1 minute for tests with high back pressure).

During the two phases, the flow rates are controlled as follow:

- "on" phase: $Q_{fuel} = Q_{\lambda,fuel}$ and $Q_{ox} = Q_{\lambda,ox}$
- "off" phase: $Q_{fuel} = Q_{fuel,\ min\ flow}$ and $Q_{ox} = Q_{ox,\ min\ flow}$

Where Q_i = is the flow of flow "i", $Q_{\lambda,i}$ is the stoichiometric flow, and $Q_{i,min\ flow}$ is the minimum flow. Min flow is set to 0.05Nl/min for both the cathode and anode flow. The stoichiometries are set to 1.25 and 2.5 at the anode and cathode respectively.

The on/off cycling is stopped after a total duration of approximately 240 hours or if the cell voltage drops below 0.2 V.

6.5 End of period measurements

6.5.1 Polarization measurements

The cell polarization is examined in ascending current control mode (from low to high current densities) shortly after the ageing period is ended (23 hours with on/off cycling). The current density range was between 0 and 1.0 A cm^{-2}, with a delay of 60 s at each current setting (to avoid voltage drops when changing current settings the flow corresponding to the next current step is applied during the last 60 s at each step). The duration of each current setting is: 3 min for i<0.1 A cm^{-2} and 5 min for 0.1<i<1.0 A cm^{-2}. Before each of the polarization measurements, a short state of constant current mode is performed (0.5 A cm^{-2}). To avoid irreversible damage of the cell components the polarization measurements are stopped when the maximum current density is reached or when the cell voltage goes below 0.2 V.

The final polarization curve is compared with the initial curve to quantify the loss in performance of the cell on the entire range of current densities in order to analyze the causes of degradation.

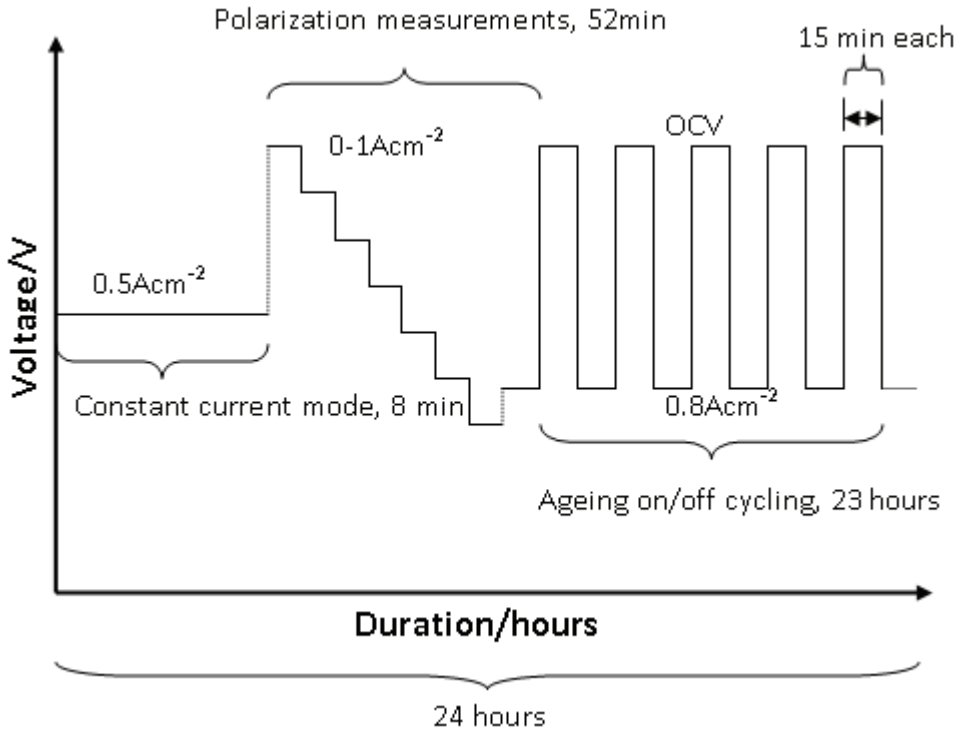

Figure 19 Test procedure after pre-conditioning of test cell. Total duration for the on/off cycle is 23 hours. The cycle is repeated 10 times giving a total duration of 240 hours.

6.5.2 Impedance test

Cell impedance tests were implemented using a fuel cell test station with an AC-impedance system. Sinusoidal current waves were emitted through the cell and shunt. By examining the voltage drop over the shunt, the complex resistance of the fuel cell electrodes can be calculated. Nyquist plots were generated by the software. From these plots, the values of resistance and capacitances in the fuel cell electrodes were determined.

6.5.3 Cyclic voltammetry

CV measurements were conducted to evaluate the cathode electrochemical active surface. The electrochemical active surface was measured by purging H_2 through the anode and N_2 through the cathode with flow corresponding to a load of 0.8 Acm^{-2} (stoic at 1.25 and 2.5 at the anode and cathode respectively).

6.5.4 Hydrogen crossover

Hydrogen crossover was measured by switching the cathode gas flow from air to pure nitrogen. The flow rate was set corresponding to a load of 0.8 V. After approximately 40 minutes of gas equilibration, a potentiostatic assessment at 0.8 V was conducted to measure the current through the fuel cell. The measured current corresponds to the oxidation of the hydrogen molecules at the cathode side in the presence of platinum catalyst.

6.5.5 Effluent analysis

In order to examine the degree of chemical degradation in the membrane ionomer, the fluoride concentrations of the cathode and anode outlet water were evaluated. Water samples were collected in plastic jars after each of the aging cycles. The jars were washed before use by deionized water for three times. An ion chromatograph at SINTEF was used to analyze the water samples.

7 Results and discussion

7.1 Introduction

A total number of 6 tests were performed, including one replicate of Test 1 and Test 3.

The different tests were performed in random order. Table 5 shows the different tests in the performed order.

Test no.	Relative humidity/%	Clamping pressure/barg	Back pressure/barg	Level		
Test 3	100	5	0	+	-	-
Test 1	25	5	1.5	-	-	+
Test 4	100	10	1.5	+	+	+
Test 2	25	10	0	-	+	-

Table 5 Performed order of the tests with the belonging operating conditions.

Cyclic voltammetry, impedance and hydrogen crossover measurements were attempted carried out on the first tests. However, due to inexplicable cell failure during the measurements, all experiments discussed below were performed without electrochemical measurements (except replicate of Test 1).

7.2 Initial performance

In order to compare performance and durability for the four different tests the initial performance were examined. After pre-conditioning, the cell was run at constant current density (0.5 A cm^{-2}) before setting the operating conditions. Table 6 shows an averaged value of the voltage response for the four different tests.

Initial performance: i= 0.5 A cm^{-2}		
Test	**Voltage response/V**	**Ohmic resistance/Ohm cm^2**
Test 1	0.710	0.174
Test 2	0.718	0.204
Test 3	0.706	*
Tets 3 replicate	0.684	0.194
Test 4	0.708	0.205

Table 6 Voltage response to 0.5 A cm^{-2} after pre-conditioning. All values are averaged. Standard deviation for the voltage response is 5 mV. *Due to problems with the relay during Test 3 the ohmic resistance could not be obtained.

Considering variation in data measurement and differences in assembling the fuel cell a standard deviation of 5 mV is satisfying.

7.3 Durability

7.3.1 On/off cycling

The voltage profile of Test 3 for the first hour of four cycles is shown in Figure 20.

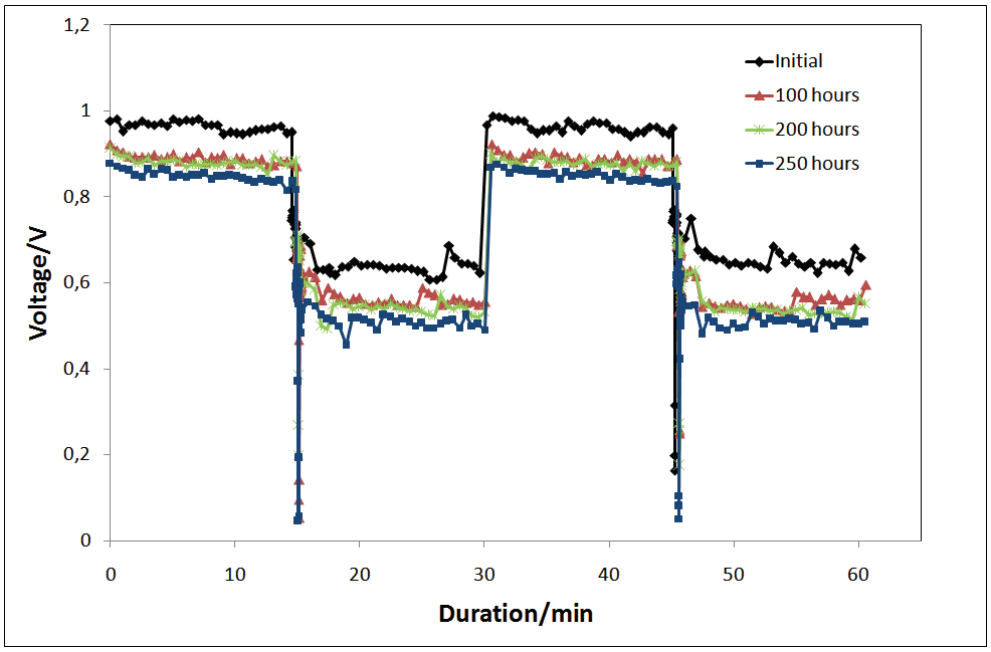

Figure 20 Voltage profile of Test 3, showing 60 minutes of the current ageing process at four different stages.

It can be seen that the OCV and the voltages needed to maintain the current density at 0.8 A cm^{-2} decreases with time. The most significant drop in the voltage profile is during the first 100 hours.

Figure 21 shows the voltage profile for Test 1. The cell showed pinhole formation between 50 and 100 hours observed by loss of OCV. The experiment was aborted after 200 hours when the OCV fell below 0.2 V.

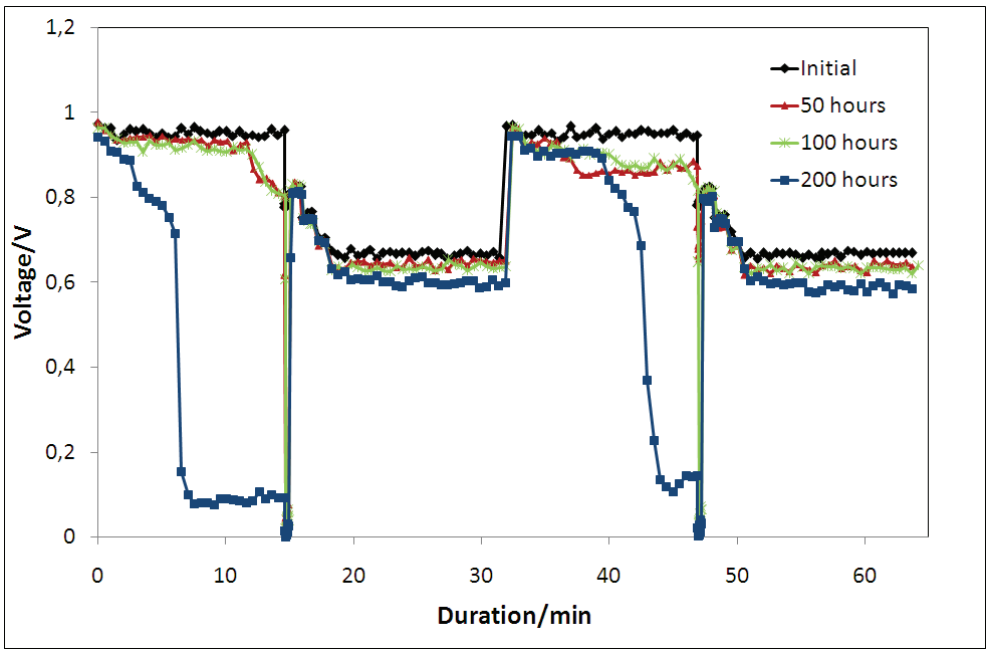

Figure 21 Voltage profile of Test 1, showing 60 minutes of the current ageing process at four different stages.

Visual examination of the used MEA gave evidence of pinhole formation. In addition, pinhole formation was observed in the replicate of Test 1 (see Appendix C Figure 38) between 50 and 70 hours.

The voltage profile for Test 4 is shown in Figure 22. Compared to Test 3, Test 4 shows a more uniform degradation.

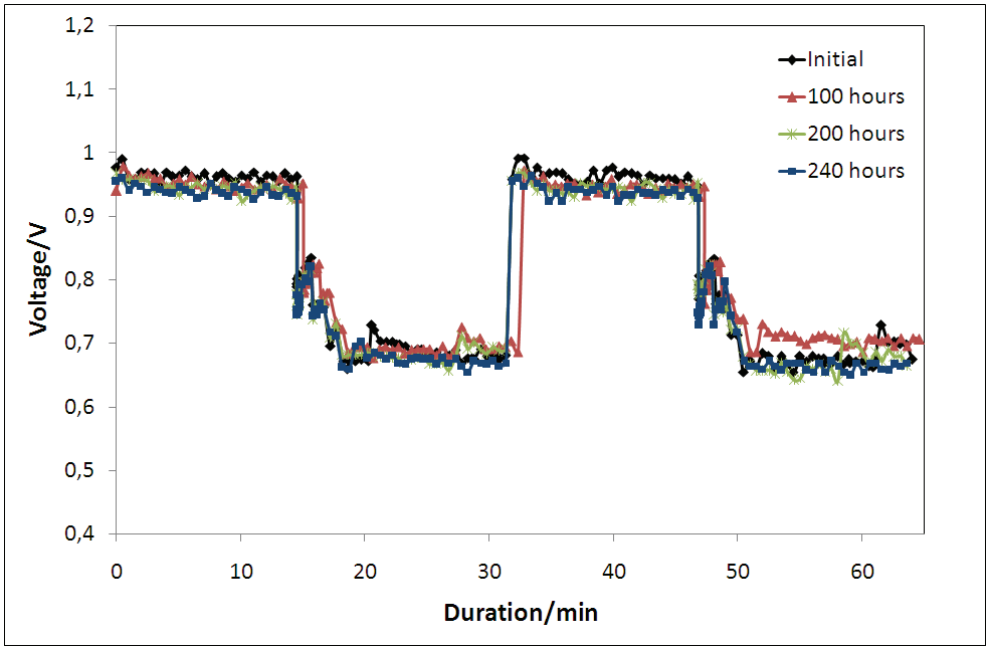

Figure 22 Voltage profile of test 4 showing 60 minutes of the current ageing process at four different stages.

Test 2 had a lifetime of less than 24 hours and was aborted when the cell failed to sustain 0.2 V at 0.8 A cm^{-2} (see Figure 23).

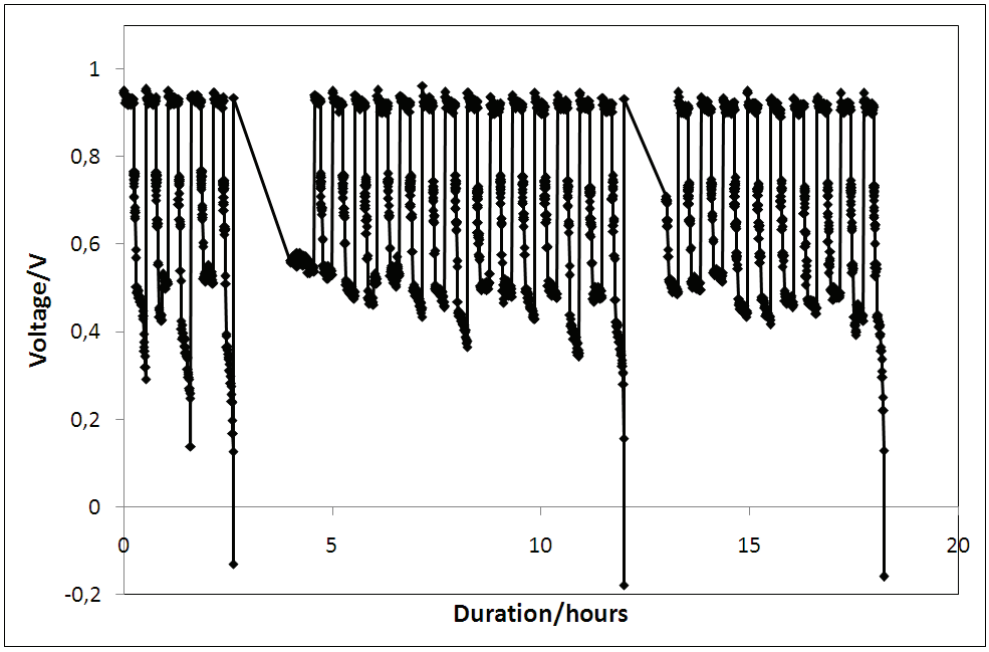

Figure 23 Ageing on/off cycling for Test 2 showing problems sustaining the voltage above 0.2 V at 0.8 A cm^{-2}. Cell was aborted after failing three times within the first 24 hours.

After the cycling was aborted the cell was run at constant current density (0.8 A cm^{-2}). Failure was observed by significant increase in cell resistance (see Figure 39 in Appendix C). The increasing resistance could be explained by dry membrane conditions which again would lead to loss in ion conductivity. The high ohmic resistance for Test 2 could also be seen from Table 9 in section 7.3.3 which contains an averaged value of the ohmic resistance during the on/off cycling. No pinhole formation was observed by visual examination of the used MEA.

In Figure 36 and Figure 37 in Appendix C the changes in temperature and pressure during on/off cycling for Test 1 is shown. These changes are observed for all tests and could obviously induce degradation both in form of chemical and mechanical failures. Changes in temperature, pressure and relative humidity could cause stresses in the membrane propagating small tears and eventually cell failure. This could be one of the reasons for the early pinhole formation for Test 1.

7.3.2 Performance

The initial polarization curves for the four different tests are shown in Figure 24. All values are an average of the last minute at each current step.

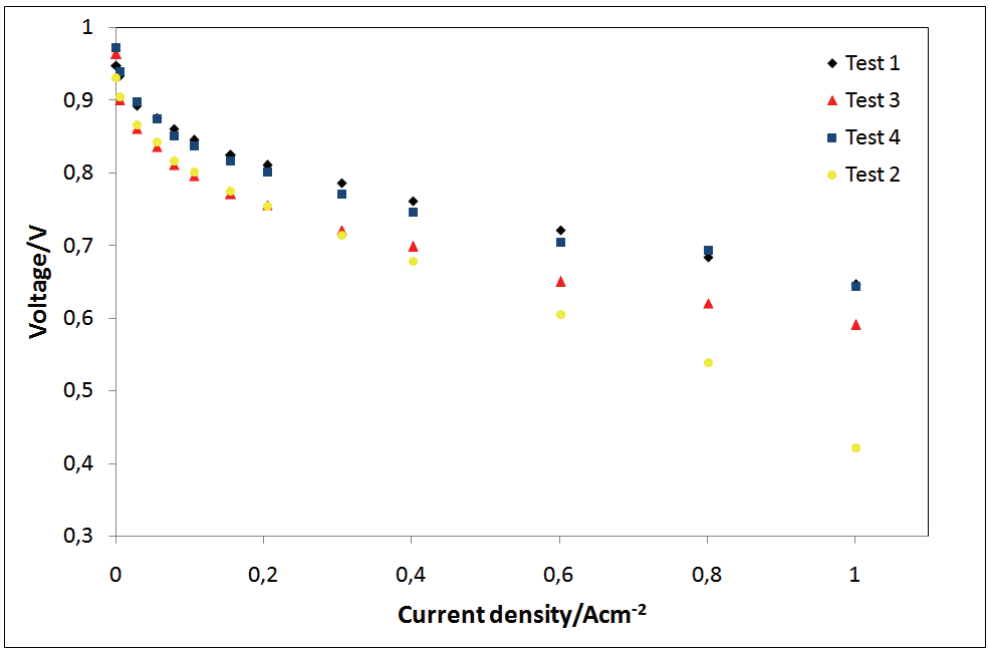

Figure 24 Initial polarization curves for the four different tests.

Figure 24 shows how the performance of Test 1 and Test 4 are initially higher than for the two other tests. The improved performance is mainly due to pressurized operation.

From examination of the kinetics, ohmic and mass transport regions of the polarization curves it can be seen that Test 2, and to a certain extent Test 4, have mass transport limitations at high current densities. This could be explained by the high clamping pressure. However, the actual clamping pressure on the active area for Test 4 would be lower than for Test 2 due to the high back pressure. The increasing loss of performance at increasing current densities of Test 2 could be explained by high ohmic resistance. This is discussed in more detail in section 7.3.3.

Figure 25 shows the polarization curves after 192 hour of duration. Due to problems with the potentiostat in Test 3 the current density could not reach 1 A cm^{-2}. Since Test 2 failed before 24 hours Test 2 is not included in this figure.

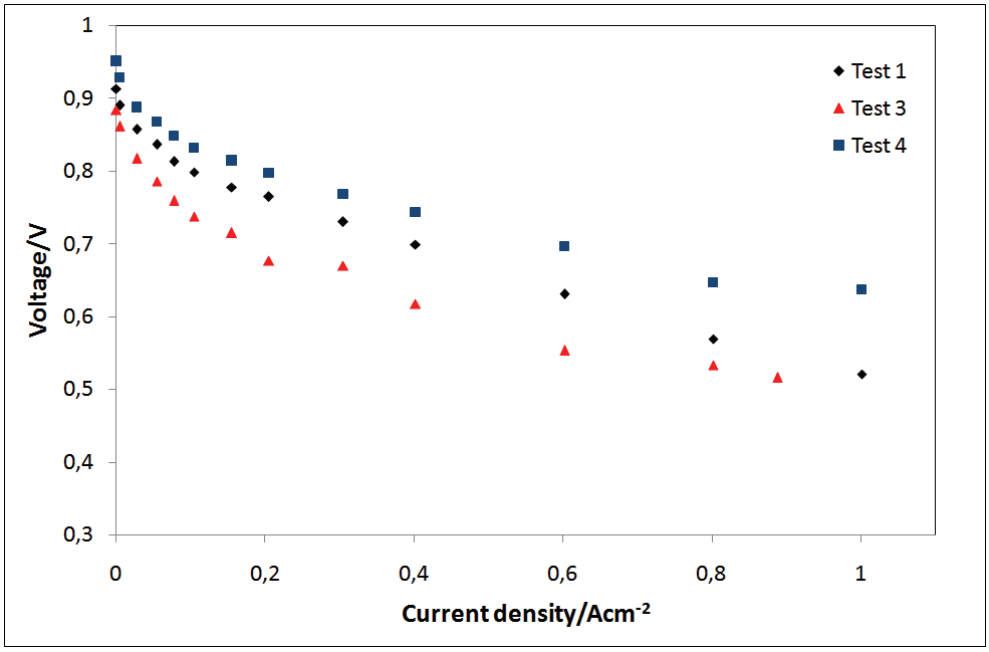

Figure 25 Polarization curves after 192 hours of duration.

From examination of the kinetics, ohmic and mass transport regions of the polarization curves for Test 4, it is clear the most significant degradation that occurred was the lowering of the OCV. The slopes of the curves at the ohmic and mass transport regions were similar during the 192 hour duration. The test with the most significant performance loss is Test 1 which could be explained by high crossover and chemical degradation due to pinhole formation.

Figure 26 shows the voltage decay of Test 1, 3 and 4. This shows that the cell (Test 1) operated with low humidity (25 %) has the most significant voltage loss which is increasing with increasing current densities. The most significant degradation of Test 3 and 4 could again be seen in loss of OCV.

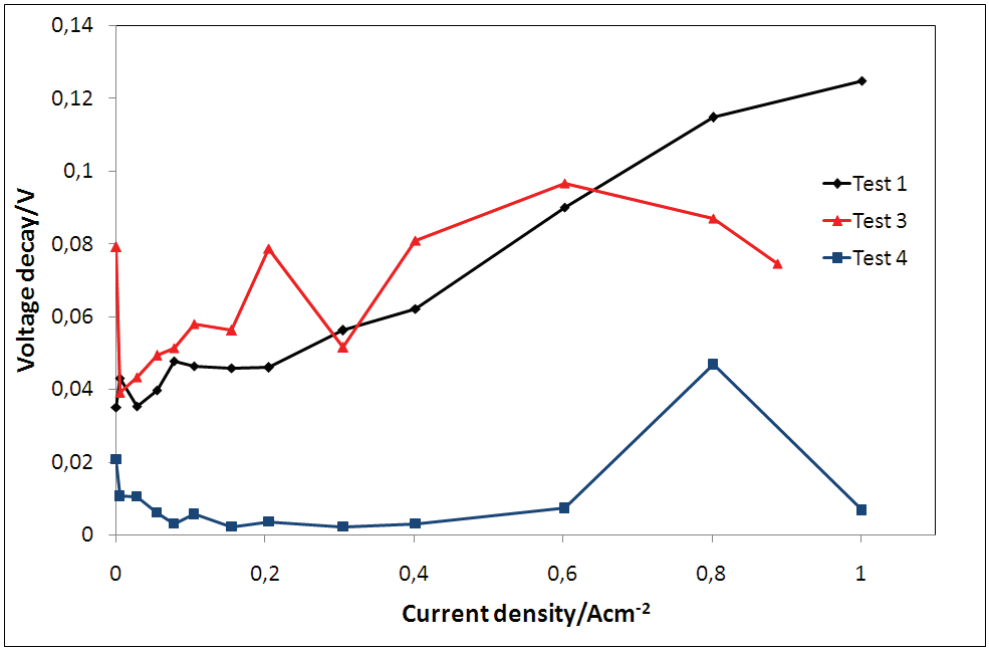

Figure 26 Voltage decay calculated from the initial and 192 hour polarization curves.

All tests showed an increasing voltage loss with increasing current densities. This could be explained by increased mass transport limitations. Increased mass transport limitations could be promoted by degradation of GDL (loss of hydrophobicity) and/or by loss in active area. Cyclic voltammetry measurements were performed on the replicate of Test 1 showing loss in active area during the first 96 hours of ageing on/off cycling (see Appendix E Figure 42).

To evaluate the voltage decay for each test in a way that is comparable the ageing on/off cycle results were used. Table 7 shows an average of the last 5 min of the three first steps at different periods in the on/off cycle.

Test 1 ("- - +")			Test 3 ("+ - -")			Test 4 ("+ + +")		
Duration	OCV	0.8 Acm^{-2}	Duration	OCV	0.8 Acm^{-2}	Duration	OCV	0.8 Acm^{-2}
0	0.951	0.664	0	0.956	0.640	0	0.959	0.677
25	0.879	0.637	25	0.889	0.545	25	0.954	0.689
50	0.889	0.648	50	0.888	0.564	50	0.953	0.704
100	0.881	0.637	100	0.870	0.540	100	0.944	0.703
150	0.301	0.615	150	0.866	0.528	150	0.942	0.676
200	0.419	0.598	200	0.860	0.503	200	0.941	0.683

Table 7 Voltage response during 200 hours of on/off cycling. All values are an average of the last 5min of the 3 first steps at the actual time.

The least squares regression method for the data in Table 7 is then used to calculate an overall voltage loss. Table 8 shows the calculated voltage loss with the corresponding standard deviation for the slope.

	OCV		0.8Acm-2	
Test no.	Voltage loss/µVh^{-1}	STD	Voltage loss/µVh^{-1}	STD
Test 1	3184	9.00E-04	287	5.08E-05
Test 3	360	1.39E-04	500	1.70E-04
Test 4	91.7	1.41E-05	28.9	7.75E-05

Table 8 Voltage loss calculated from data from the ageing on/off cycling.

It can be seen from Table 8 that the test with low humidity (Test 1) has the highest loss in OCV. This is mainly due to pinhole formation which would lead to crossover. In addition the high back pressure and the difference in anode and cathode back pressure during OCV (see Figure 37 in Appendix C) would increase the crossover rate.

Comparing the two tests with 100 % relative humidity, the voltage loss for both OCV and 0.8 A cm^{-2} for Test 3 is significantly higher, even greater than for Test 1.

Both experiments with low humidity (Test 1 and Test 2) showed inferior durability. Test 1 failed due to pinhole formation and Test 2 due to dry membrane condition observed by increasing ohmic resistance. One possible explanation to the different failure modes could be the difference in back pressure. In the situation with low humidity; high back pressure would reduce the problems with dry membrane conditions. This could also be seen from the initial polarization curves in Figure 24 where Test 2 has a distinct loss in the mass transport region. The high back pressure in Test 1 would lead less water out of the cell (due to the reduction of volumetric flow), hence reducing the ohmic resistance as the current density increases.

7.3.3 Ohmic resistance

An averaged value of the ohmic resistance during the ageing on/off cycling is listed in Table 9. Comparing the ohmic resistance of the four tests shows high values for the two cells with 25 % relative humidity.

Test	Ohmic resistance/Ohm cm^2
Test 1 ("- - +")	0.125
Test 2 ("- + -")	0.256
Test 3 replicate	0.103
Test 4 ("+ + +")	0.095

Table 9 Ohmic resistance during on/off cycling between 100-150 hours. (Averaged values). Test 2 failed before 24 hours and is an averaged value from the first 24 hours.

Due to problems with the relay in Test 3 the ohmic resistance for the replicate is used. It is evident from these results that humidification is essential for reduction of the ohmic resistance.

To illustrate the effect of high ohmic resistance the initial polarization curve for Test 2 is compared with an iR corrected polarization curve (voltage response + i·R). This is shown in Figure 27.

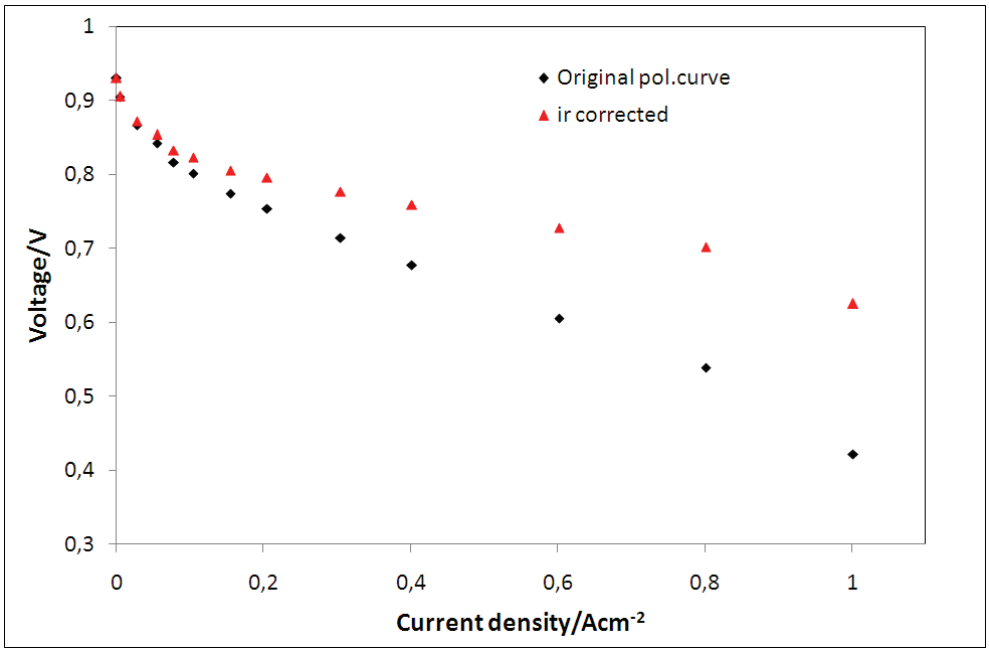

Figure 27 Initial and iR corrected polarization curve for Test 2.

Correcting the polarization curve for ohmic losses elevates the voltage at high current densities up to 0.2 V. Comparing this polarization curve with the three other initial polarization curves explains the difference in initial performance.

Figure 28 shows an averaged value of the ohmic resistance during on/off cycling for the four different tests. Generally the ohmic resistance is decreasing with time, which could indicate physical thinning of the membrane. Test 2 showed a high and increasing resistance during the 20 hour of duration.

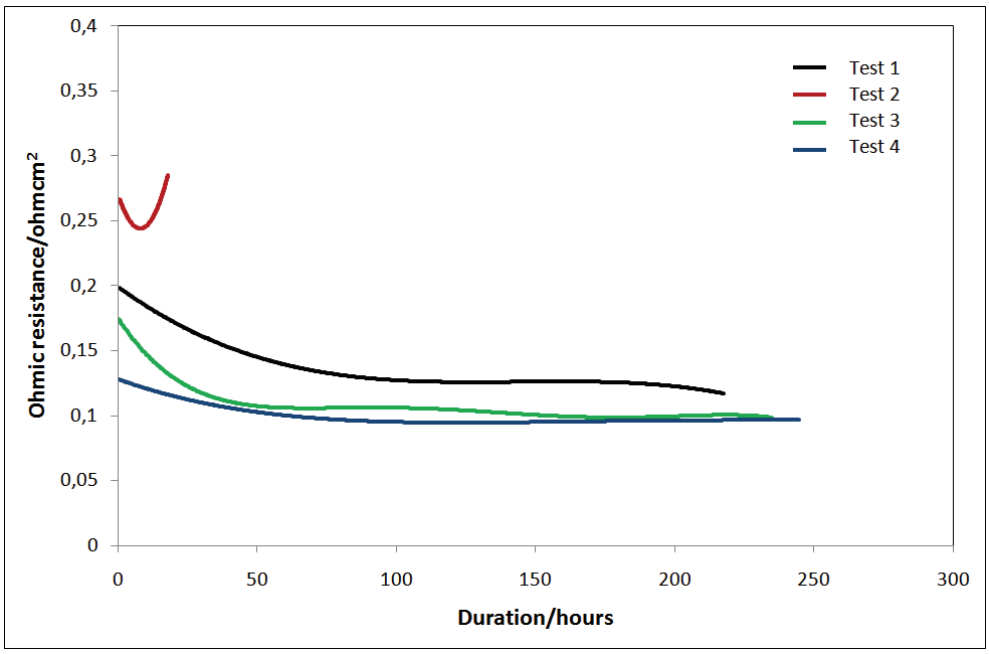

Figure 28 The average ohmic resistance for all four tests during the ageing on/off cylcle.

7.4 Effluent analysis

Figure 29 shows the measured fluoride emission rates collected from the water samples.

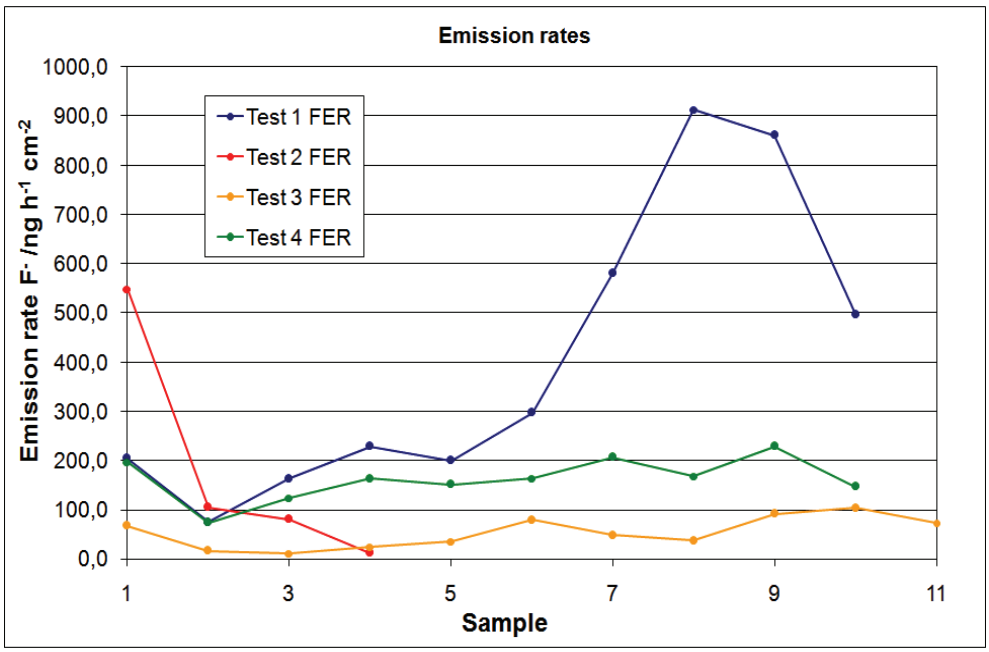

Figure 29 Measured fluoride emission rates.

Generally FER decreases after the break in procedure (Sample no. 1). This could be due to the high current densities during break in. After sample 1 the fluoride emission rates show an increasing trend with time. Higher rates are observed at the cathode (not shown in the figure). For the experiment with low relative humidity (25%), high clamping pressure (10barg) and no back pressure (Test 2), the FER is decaying. As the time of this experiment

was less than 24 hours, the effluents analyzed are more frequent and not directly comparable to the other with respect to time.

For both experiments with high humidity setting, FER is significantly lower than for Test 1 (25% relative humidity). The reason to the extremely high levels for Test 1 could be a high crossover rate resulting in accelerated chemical attack of the MEA.

Comparing the two tests with 100% relative humidity, Test 3 has lower FER than Test 4. This could be explained by the difference in back pressure which results in increased crossover.

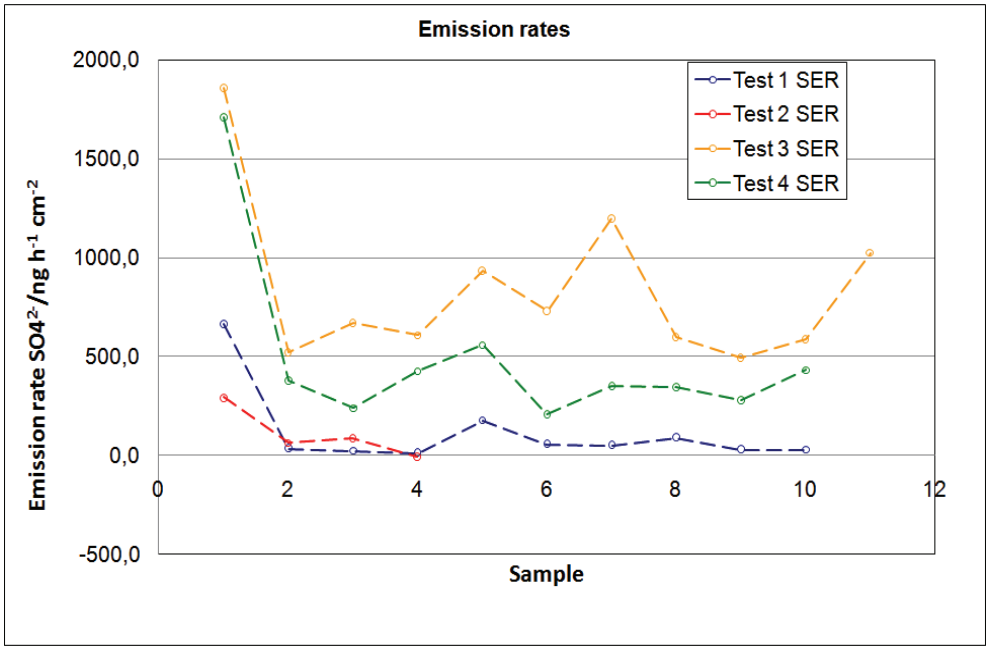

Figure 30 Measured sulfate emission rates.

As seen from Figure 30, the initial SER is high for all four experiments. It is also observed that the SER is higher at the anode (not included in the figure). Unlike earlier similar studies [34] the SER is sustained at high levels for the experiments with high humidity level. The sustained high levels of sulfur are probably a result of sulfuric acid residue from production of the MEA and/or GDLs. High humidification of gases appears to more effectively wash out the sulfur.

7.5 Correlation

Considering the observations and analysis of the results presented above, it is evident that back pressure has a positive impact on degradation both for low and high humidity levels. It is difficult to extract the effect of clamping pressure, however it seems like high clamping pressure could promote mass transport limitations. This could be explained by deformation of the MEA and/or GDL changing the materials mass transfer properties. Deformation of the GDL could result in loss of the hydrophobic properties. This could result in local flooding which again would limit mass transfer, especially at high current densities.

From the tests performed in this study the test (Test 4) with the best performance also shows the best durability. However, Test 1 initially showed the same performance as Test 4, but suffered from early failure observed by pinhole formations and was aborted after 200 hour of duration.

7.6 Replicates

7.6.1 Durability

Figure 31 compares the polarization curve after 192 hours of duration for test 3 and the replicate. The figure shows a satisfying variance in performance. It can be seen from Figure 43 in Appendix D that like test 3 the replicate test also shows the most significant drop in voltage response during the first 100 hour of duration.

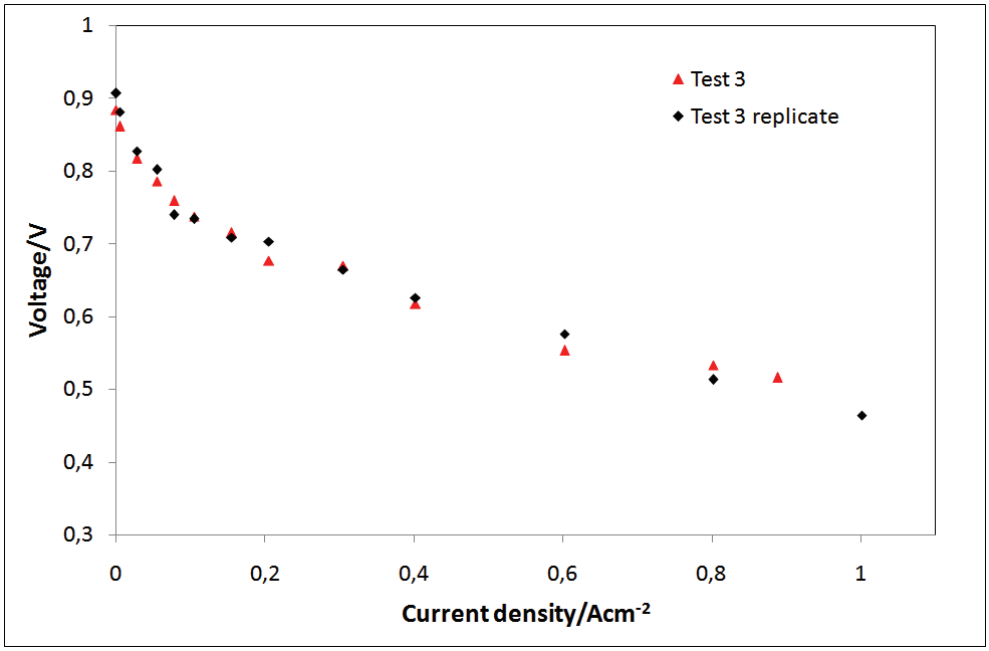

Figure 31 Polarization measurements after 192 hour of duration for test 3 and the replicate of test 3.

Like Test 1 the replicate of Test 1 showed pinhole formation between 50 – 100 hours. The voltage response during on/off cycling for the replicate is shown in Appendix D Figure 40.

7.6.2 Effluent analysis

Figure 32 shows the measured fluoride and sulfate emission rates for Test 1 and the replicate of Test 1. Both experiments show high and increasing FER rates. SER rates are initially high and decreasing. It can be seen from the figure that the variation in SER measurements are small.

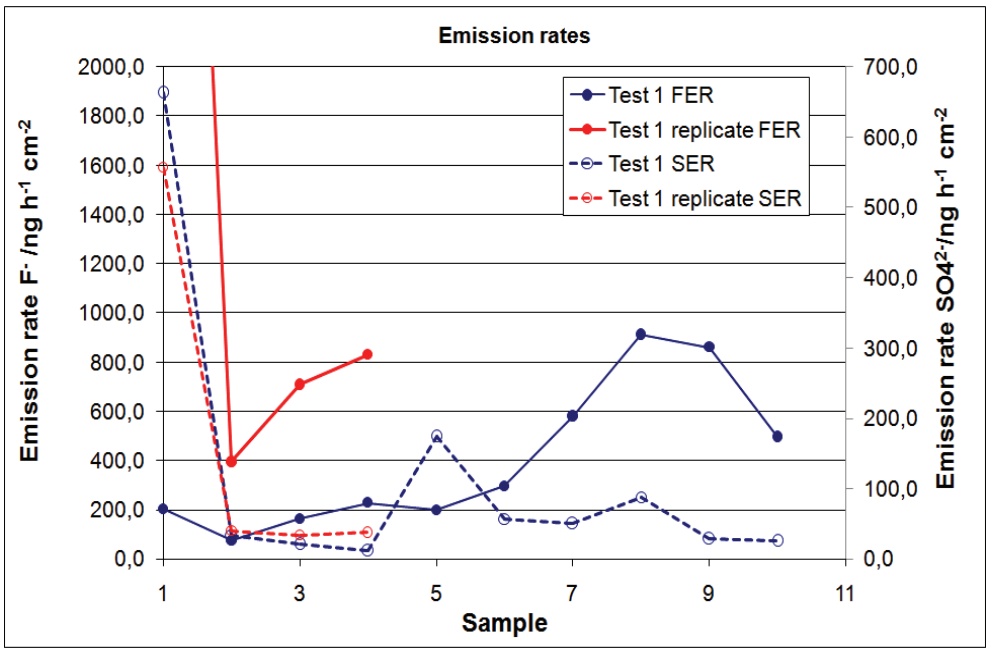

Figure 32 Measured fluoride and sulfate emission rates for Test 1 and Test 1 replicate.

Figure 33 shows the fluoride and sulfate emission rates for Test 3 and Test 3 replicate. Both tests show similar trends during 240 hour of duration. The variation in FER and SER are acceptable.

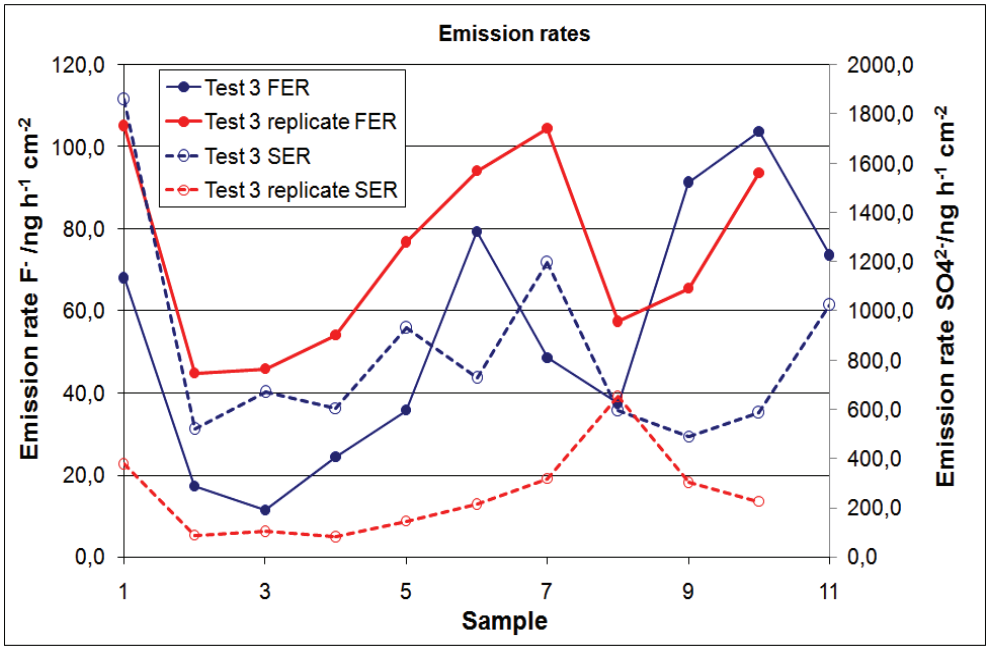

Figure 33 Measured fluoride and sulfate emission rates for Test 3 and Test 3 replicate.

8 Conclusion

The most favorable combination of operating conditions considered in this study are 100 % relative humidity, 10 barg clamping pressure and 1.5 barg back pressure (Test 4). This combination showed both best performance and lowest degradation rates.

The tests with low humidification levels showed inferior durability. Test 1 showed pinhole formation between 50 and 100 hours observed by significant loss of OCV. Test 2 had a lifetime of less than 24 hours and failure was observed by significant increase in ohmic resistance. Generally the cells have increasing voltage loss with increasing current densities.

Back pressure had a positive effect on both performance and durability. The effect of clamping pressure was difficult to extract from the performed tests, however high clamping pressure seems to lead to increased mass transport limitations.

The effluent analysis shows a strong dependence on humidification levels. Generally the FER shows an increasing trend with time while SER are sustained at high levels. Cell failure is not observed by altered emission rates.

9 Recommendations for future work

To find a clear correlation between humidification and pressures the designed test matrix (2^{3-1}) should be completed (a 2^3 design). The two experiments with low relative humidity should be replicated with cyclic voltammetry and impedance measurements to examine loss of active area and crossover rates.

Test 3 and Test 4 should be replicated with cyclic voltammetry to examine loss in active area. In addition the experiment with 100 % relative humidity, high clamping pressure and no back pressure ("+ + -") should be performed to supplement the effect of high relative humidity.

In the present work manual pressure regulators were used, which caused variations in pressure during the on/off cycling. It is therefore recommended that future tests use electronic regulated pressure regulators.

In order to obtain better temporal resolution, SINTEF has designed automated water samplers that render emission analysis possible every two hours. Future work should attempt to use this system.

This work addressed operation on pure hydrogen only. From the point of view of automotive applications, performance and durability on CO-containing and dilute feeds should be considered in future work.

References

1. Energy, D.O., *Basic research needs for the hydrogen economy*. 2003. p. 56-57.
2. Zawodzinski, T.A., et al., *Characterization of polymer electrolytes for fuel cell applications.* Solid State Ionics, 1993. **60**(1-3): p. 199-211.
3. Dicks, L., *Fuel Cell System Explained*. Second Edition ed. 2006, Chichester, England: Wiley.
4. Yan, Q., H. Toghiani, and J. Wu, *Investigation of water transport through membrane in a PEM fuel cell by water balance experiments.* Journal of Power Sources, 2006. **158**(1): p. 316-325.
5. Chang, W.R., et al., *Effect of clamping pressure on the performance of a PEM fuel cell.* Journal of Power Sources, 2007. **166**(1): p. 149-154.
6. Borup, R.L., et al., *PEM fuel cell electrocatalyst durability measurements.* Journal of Power Sources, 2006. **163**(1): p. 76-81.
7. Antolini, E., *Formation, microstructural characteristics and stability of carbon supported platinum catalysts for low temperature fuel cells.* Journal of Materials Science, 2003. **38**(14): p. 2995-3005.
8. Maass, S., et al., *Carbon support oxidation in PEM fuel cell cathodes.* Journal of Power Sources, 2008. **176**(2): p. 444-451.
9. Shao, Y., G. Yin, and Y. Gao, *Understanding and approaches for the durability issues of Pt-based catalysts for PEM fuel cell.* Journal of Power Sources, 2007. **171**(2): p. 558-566.
10. Ohma, A., S. Yamamoto, and K. Shinohara, *Membrane degradation mechanism during open-circuit voltage hold test.* Journal of Power Sources. **In Press, Corrected Proof**.
11. Jeremy, P.M. and M.D. Robert, *Model of Carbon Corrosion in PEM Fuel Cells*. 2006, ECS. p. A1432-A1442.
12. Jian, X., et al., *Microstructural Changes of Membrane Electrode Assemblies during PEFC Durability Testing at High Humidity Conditions*. 2005, ECS. p. A1011-A1020.
13. Knights, S.D., et al., *Aging mechanisms and lifetime of PEFC and DMFC.* Journal of Power Sources, 2004. **127**(1-2): p. 127-134.
14. Bett, J.A.S., K. Kinoshita, and P. Stonehart, *Crystallite growth of platinum dispersed on graphitized carbon black : II. Effect of liquid environment.* Journal of Catalysis, 1976. **41**(1): p. 124-133.
15. Kinoshita, K., J.T. Lundquist, and P. Stonehart, *Potential cycling effects on platinum electrocatalyst surfaces.* Journal of Electroanalytical Chemistry, 1973. **48**(2): p. 157-166.
16. Liu, W. and D. Zuckerbrod, *In situ detection of hydrogen peroxide in PEM fuel cells.* Journal of The Electrochemical Society, 2005. **152**: p. 1165-1170.
17. Mittal, V.O., H.R. Kunz, and J.M. Fenton, *Is H_2O_2 involved in the membrane degradation mechanism in PEMFC?* Electrochimical and Solid-State Letters, 2006. **9**(6): p. 299-302.
18. Yeager, E., *Dioxygen electrocatalysis: mechanisms in relation to catalyst structure.* Journal of Molecular Catalysis, 1986. **38**(1-2): p. 5-25.

19. Kinumoto, T., et al., *Durability of perfluorinated ionomer membrane against hydrogen peroxide.* Journal of Power Sources, 2006. **158**(2): p. 1222-1228.
20. Hommura, S., et al., *Development of a method for clarifying the perfluorosulfonated membrane degradation mechanism in a fuel cell environment.* Journal of The Electrochemical Society, 2007. **155**(1): p. A29-A33.
21. J.St-Pierre, et al., *Relationships between water management, contamination and lifetime degradation in PEFC.* Journal of New Materials for Electrochemical Systems, 2000. **3**: p. 99-106.
22. Endoh, E., et al., *Degradation Study of MEA for PEMFCs under Low Humidity Conditions*. 2004, ECS. p. A209-A211.
23. Pozio, A., et al., *Nafion degradation in PEFCs from end plate iron contamination.* Electrochimica Acta, 2003. **48**(11): p. 1543-1549.
24. Rod Borup, e.a. and et al., *Scientific Aspects of Polymer Electrolyte Fuel Cell Durability and Degradation*. 2007.
25. Tang, Y., et al., *An experimental investigation of humidity and temperature effects on the mechanical properties of perfluorosulfonic acid membrane.* Materials Science and Engineering: A, 2006. **425**(1-2): p. 297-304.
26. Cheng, X., et al., *A review of PEM hydrogen fuel cell contamination: Impacts, mechanisms, and mitigation.* Journal of Power Sources, 2007. **165**(2): p. 739-756.
27. Ødegård, A., *Forberedelse til syklisk voltammetri (CV) forsøk i SEP*. 2006, SINTEF Materialer og kjemi: Trondheim. p. 5.
28. Zhu, W.H., R.U. Payne, and B.J. Tatarchuk, *PEM stack test and analysis in a power system at operational load via ac impedance.* Journal of Power Sources, 2007. **168**(1): p. 211-217.
29. Team, T.U.S.D.a.F.C.F.C.T., *DOE cell component accelerated stress test protocols for PEM fuel cells*. 2007.
30. Ofstad, A.B., *Flow scheme for fuel cell test station*. 2007, SINTEF Material and Chemistry: Trondheim, Norway.
31. Møller-Holst, S., *Solid Polymer Fuel Cells, Electrode And Membrane Performance Studies*, in *Institutt for fysikalsk kjemi*. 1996, NTNU: Trondheim.
32. George E.P Box, J.S.H., William G. Hunter, *Statistics for experimenters*. Second Edition ed, ed. Wiley-Interscience. 2005, New Jersey: John Wiley & Sons, Inc.
33. Sørli, J.G.H., *Development and testing of a new PEMFC design*. 2007, Department of Energy and Process Engineering: Trondheim, Norway. p. 52.
34. Aarhaug, T.A. and A.M. Svensson, *Degradation Rates of PEM Fuel Cells Running at Open Circuit Voltage.* Electrocheimical transaction article, 2006.
35. James Larmine, A.D., *Fuel Cell Systems Explained*. Vol. Second edition. 2006, Chichester, England: Wiley. 46-66.

Appendix A: Basic equations

This appendix gives an overview of the basic thermodynamic equation concerning electrochemical energy conversion in fuel cells.

Reversible cell potential
The reversible cell potential is given by the difference between the reversible electrode potentials:

$$\mathrm{E_{rev}} = \mathrm{E_{c,rev}} - \mathrm{E_{a,rev}} \qquad \text{A.1}$$

where the subscripts a and c denote the anode and the cathode, respectively.

The reversible cell potential is related to Gibbs energy change. For a fuel cell this relationship is expressed by:

$$\Delta \mathrm{G} = -\mathrm{nFE_{rev}} \qquad \text{A.2}$$

where F is the Faraday constant and n is the number of electrons taking part in the cell reactions.

Consider the following general reaction:

$$\mathrm{aA} + \mathrm{bB} = \mathrm{cC} + \mathrm{dD} \qquad \text{A.3}$$

The Gibbs free energy change for this reaction is given by:

$$\Delta \mathrm{G} = \Delta \mathrm{G}^0 + \mathrm{RT ln}\left(\frac{a_C^c\, a_D^d}{a_A^a\, a_B^b}\right) \qquad \text{A.4}$$

where ΔG^0 is the Gibbs free energy change at standard conditions and a_i denote activities of species i (i = A,B,C,D).

The combination of A.2 and A.4 gives the Nernst equation.

$$\mathrm{E_{rev}} = \mathrm{E_{rev}^0} + \frac{\mathrm{RT}}{\mathrm{nF}} \ln\left(\frac{a_C^c\, a_D^d}{a_A^a\, a_B^b}\right) \qquad \text{A.5}$$

where E^0_{rev} is the standard reversible potential of the cell reaction.

Standard reversible cell potential
If e^- is the charge of one electron, then the charge that flows is

$$-2\ \mathrm{Ne} = -2\mathrm{F}\ (\mathrm{coulombs}) \qquad \text{A.6}$$

where N is Avogadro's number and F being the Faraday constant, or the charge of one mole of electrons. If E is the voltage of the fuel cell, then the electrical work done moving this charge round the circuit is:

$$\text{Electrical work done} = \text{charge} \times \text{voltage} = -2\text{FE (joules)} \qquad \text{A.7}$$

Since this is the reversible cell potential, the electrical work done will be equal to the Gibbs free energy released.

$$\Delta\bar{g}_f = -2F \cdot E$$

$$E^0_{rev} = \frac{-\Delta\bar{g}_f}{2F} \qquad \text{A.8}$$

$$G = H - TS$$

$$\Delta\bar{g}_f = \Delta\bar{h}_f - \Delta T\bar{s}$$

$$\Delta\bar{h}_f = (\bar{h}_f)_{H_2O} - (\bar{h}_f)_{H_2} - \frac{1}{2}(\bar{h}_f)_{O_2}$$

$$\Delta\bar{s} = (\bar{s})_{H_2O} - (\bar{s})_{H_2} - \frac{1}{2}(\bar{s})_{O_2}$$

If the product is liquid water and the temperature is 25°C the change in Gibbs free energy is:

$$\Delta\bar{g}_f = -237.2 \text{ (kJ mol}^{-1}\text{)}$$

The standard reversible cell potential is (calculated from A.8):

$$E^0_{rev} \approx 1.23 \text{ (V)}$$

From the transition state theory [35] the cathodic and anodic overpotentials are approximated by:

$$\eta_C = \frac{RT}{\frac{1}{2}nF}\log(i_{0,C}) - \frac{RT}{\frac{1}{2}nF}\log(i) \qquad \text{A.9}$$

$$\eta_A = \frac{RT}{nF}\left(\frac{i}{i_{0,A}}\right) \qquad \text{A.10}$$

The potential profile may be written:

$$E = E_{rev} - (\eta_A - \eta_C) - i(R_A - R_C + R_M) \qquad \text{A.11}$$

where $i_{0,A}$ and $i_{0,C}$ is the exchange current densities at the anode and cathode, respectively.

Pressurization of PEMFC

If the pressure is increased from P_1 to P_2 the increase in or gain in voltage is:

$$\Delta V_{gain} = C \ln\left(\frac{P_2}{P_1}\right) \text{volts}$$

To consider the power gain, we suppose a current I A and a stack of n cells. The increase in power is the given by:

$$\text{Power gain} = C \ln\left(\frac{P_2}{P_1}\right) \text{In watts}$$

Appendix B: Introductory tests

Figure 34 shows how the OCV falls when the clamping pressure is changed from 5 barg to 20 barg.

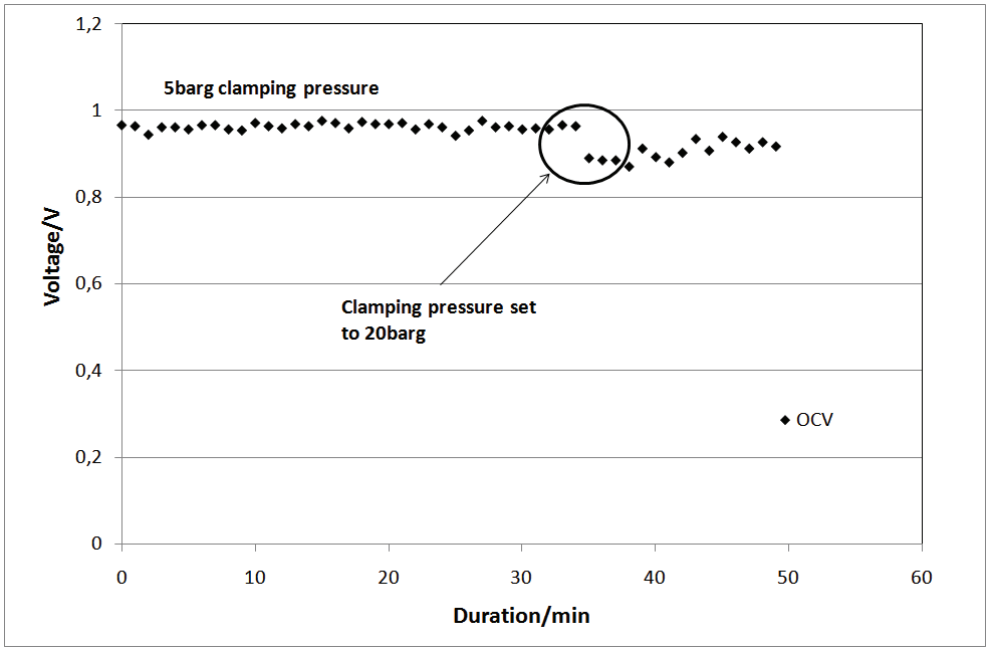

Figure 34 Testing of clamping pressure.

Figure 35 shows the first OCV step during on/off cycling. The rapid fall in OCV indicates membrane failure due to torn membrane, cracks and/or pinhole formation. Visual examination of the used MEA reveals that the high clamping pressure has torn the membrane.

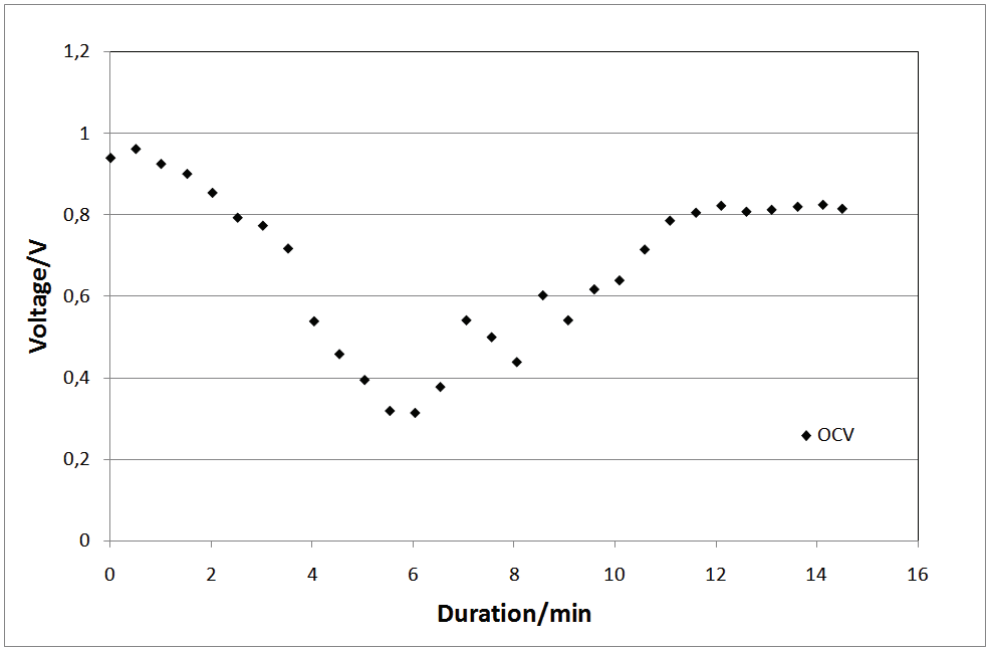

Figure 35 OCV during ON-OFF cycling. Clamping pressure at 20barg and back pressure at 1.5barg.

Appendix C: Additional results from on/off cycling

Figure 36 and Figure 37 shows how the temperature and pressure changes during on/off cycling for Test 4. Similar changes are observed for all tests.

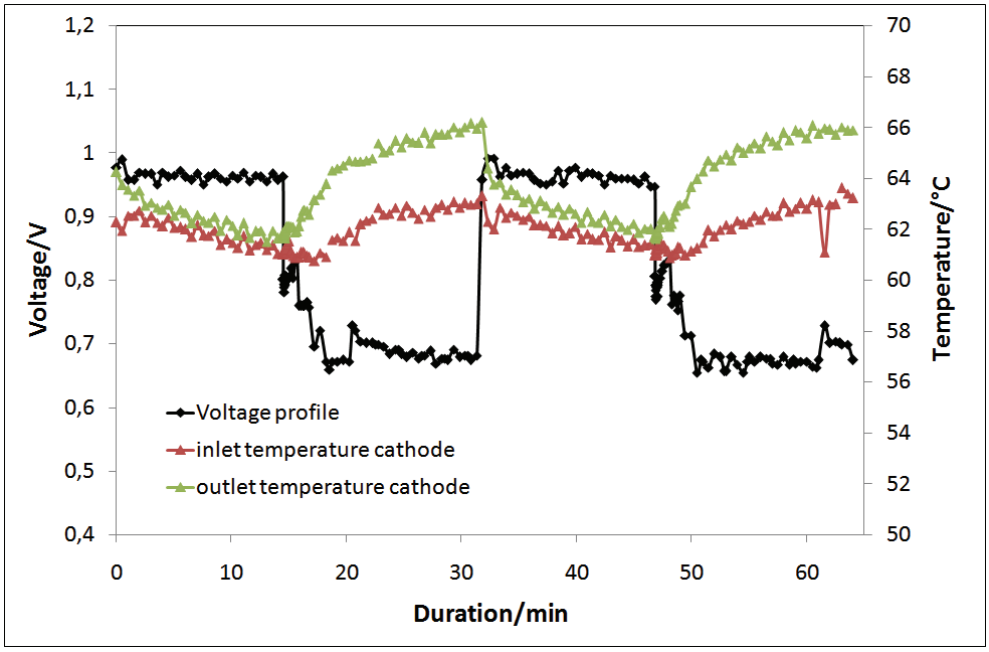

Figure 36 Change in cathode temperature during on/off cycling for Test 4.

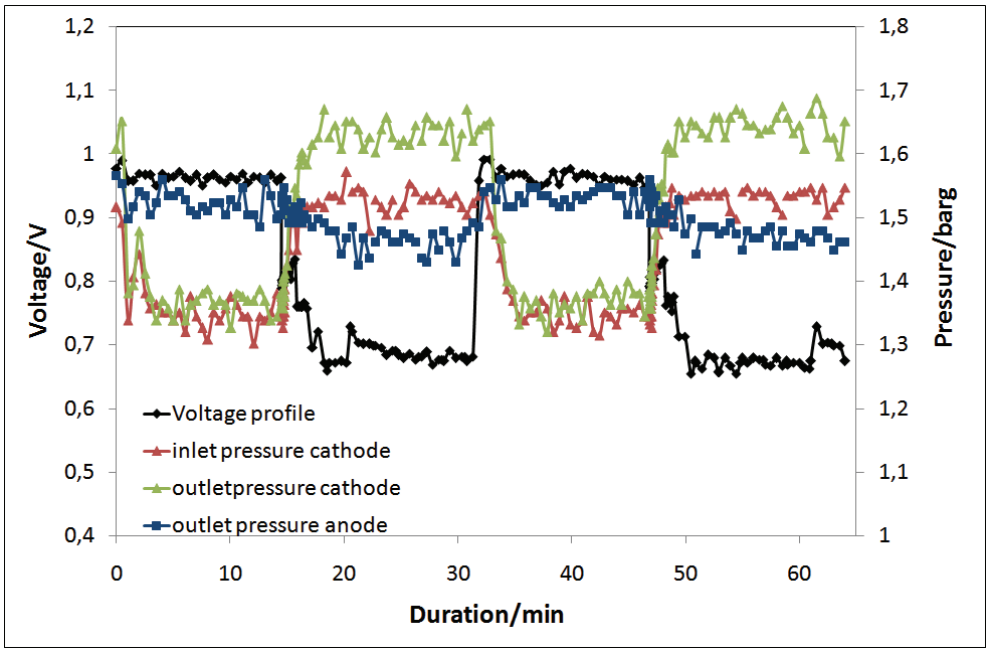

Figure 37 Change in pressure during on/off cycling for Test 4.

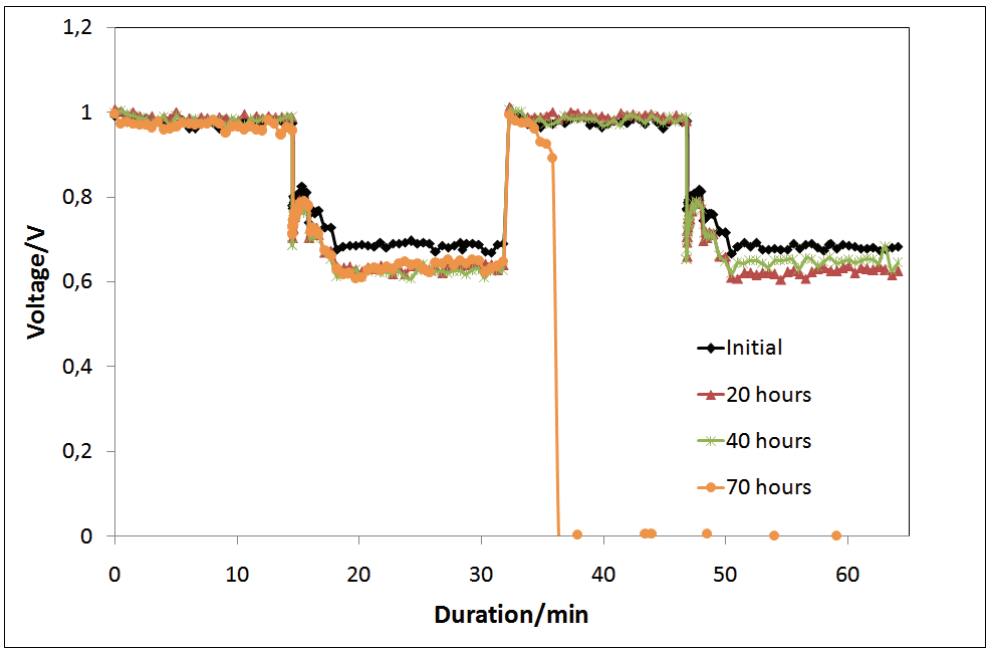

Figure 38 Voltage profile of replicate test 1 during on/off cycling revealing problems with pinhole formation.

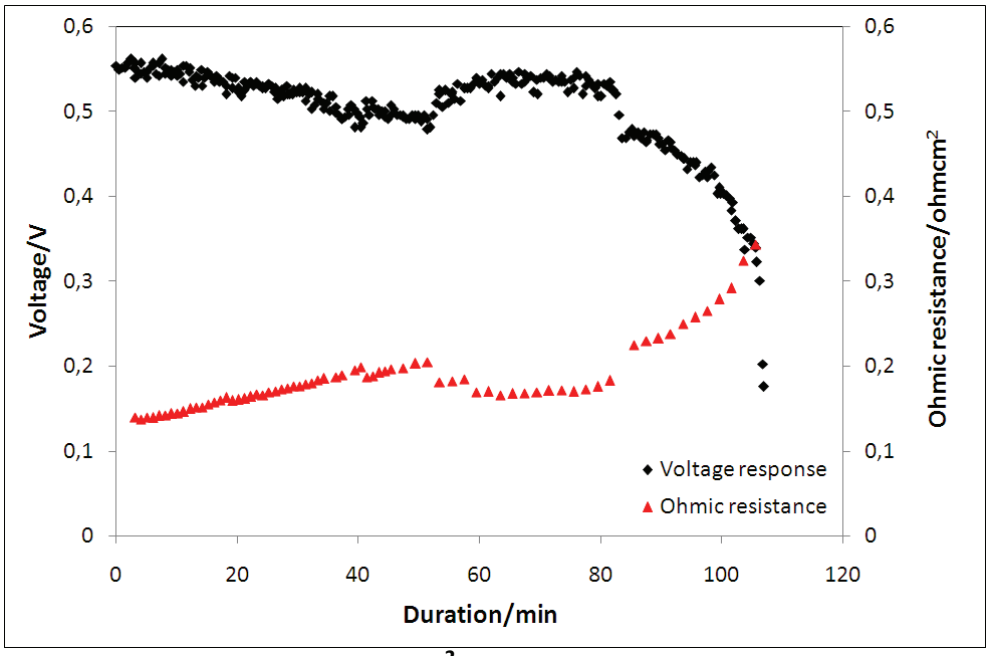

Figure 39 Test 2 run at 0.8Acm^{-2} showing cell failure and significant increase in ohmic resistance.

Appendix D: Durability test protocols

DOE CELL COMPONENT ACCELERATED STRESS TEST PROTOCOLS FOR PEM FUEL CELLS

(Electrocatalysts, Supports, Membranes, and Membrane Electrode Assemblies)

March 2007

Fuel cells, especially for automotive propulsion, must operate over a wide range of operating and cyclic conditions. The desired operating range encompasses temperatures from below the freezing point to well above the boiling point of water, humidity from ambient to saturated, and half-cell potentials from 0 to >1.5 volts. Furthermore, the anode side of the cell may be exposed to hydrogen and air during different parts of the driving and start/stop cycles.

The severity in operating conditions is greatly exacerbated by the transient and cyclic nature of the operating conditions. The cell/stack conditions cycle, sometimes quite rapidly, between high and low voltages, temperatures, humidities, and gas compositions. The cycling results in physical and chemical changes, sometimes with catastrophic results.

This document describes test protocols to assess the performance and durability of fuel cell components intended for automotive propulsion applications. The goal of this testing is to gain a measure of component durability and performance of electrocatalysts and supports, membranes, and membrane electrode assemblies (MEAs) for comparison against 2010 DOE targets contained in **Reference 1**. The resulting data may also help to model the performance of the fuel cell under variable load conditions and the effects of ageing on performance.

These protocols are intended to establish a common approach for determining and projecting the durability of polymer electrolyte membrane (PEM) fuel cell components under simulated automotive drive cycle conditions.

This document is not intended to be comprehensive as there are many issues critical to a vehicular fuel cell (e.g., freeze/thaw cycles) that are not addressed at this time. Additional issues will be addressed in the future. Furthermore, it is recognized that the cycles specified herein have not been fully correlated with data from stacks and systems operated under actual drive cycles. Therefore, additional tests to correlate these results to real world lifetimes is needed, including actual driving, start/stop, and freeze/thaw cycles.

The durability of catalysts can be compromised by platinum (Pt) sintering, particle growth, and dissolution, especially at high electrode potentials; this sintering/dissolution is accelerated under load-cycling. Durability of catalyst supports is another technical barrier for stationary and transportation applications of PEM fuel cells. Corrosion of high-surface area carbon supports poses significant concerns at high electrode potentials and is accelerated during start/stop cycles and during higher temperature operation (>100°C).

Membranes are another critical component of the fuel cell stack and must be durable and tolerate a wide range of operating conditions including low humidity (20 to 100% RH) and high

temperature (-40 to 120°C for transportation applications and >120°C for stationary applications). The low operating temperature and the humidity requirements of current membranes add complexity to the fuel cell system that impacts the system cost and durability. Improved membranes are needed that perform better and are less expensive than the current generation of polymer membranes.

The associated testing protocols and performance metrics are defined in Table 1 for electrocatalysts, Table 2 for catalyst supports, Table 3 for membrane/MEA chemical stability, and Table 4 for membrane/MEA mechanical durability, respectively, as derived from **References 2, 3, and 4**.

The specific conditions and cycles are intended to isolate effects and failure modes and are based on assumed, but widely accepted, mechanisms. For example, the electrocatalyst cycle is different from the support cycle because they suffer from different degradation mechanisms under different conditions. Similarly, membrane/MEA chemical degradation is distinguished from mechanical degradation.

Durability screening at conditions and under cycles different from those presented here-in are acceptable provided that the developer can provide:

- conclusive/convincing evidence that the cycle/conditions do not compromise separation/isolation of degradation mechanisms
- degradation rates extrapolated to the conditions/cycles prescribed here-in

Data to be reported, if applicable, at each point on the polarization curves and during steady-state and variable load operation include, but are not limited to:

- Ambient temperature and pressure
- Cell voltage
- Cell current and current density
- Cell temperature
- Cell resistance, if available (along with test conditions)
- Fuel inlet and outlet temperature
- Fuel flow rate
- Fuel inlet and outlet pressure
- Fuel inlet dew point
- Air inlet and outlet temperature
- Air flow rate
- Air inlet and outlet pressure
- Air inlet dew point
- Fuel and air quality
- Coolant inlet temperature
- Coolant outlet temperature
- Coolant flow rate

Pre-test and post-test characterization of cell and stack components should be performed according to developer's established protocols. At the discretion of the developer, tests should be terminated when hydrogen crossover exceeds safe levels.

References

1. Hydrogen, Fuel Cells & Infrastructure Technologies Program Multi-Year Research, Development and Demonstration Plan, August 2006 (http://www1.eere.energy.gov/hydrogenandfuelcells/mypp/)
2. Appendix D of DOE Solicitation **DE-PS36-06GO96017**
3. Mathias, M., et al, "Two Fuel Cells in Every Garage?" Interface Vol. 14, No 3, Fall 2005.
4. Mathias, M., et al, "Can Available Membranes and Catalysts Meet Automotive PEFC Requirements?" Presentation at ACS Meeting, Philadelphia, August 2004.

Table 1
Electrocatalyst Cycle and Metrics

Cycle	Step change: 30s at 0.7V and 30s at 0.9 V. Single cell 25 - 50cm^2	
Number	30,000 cycles	
Cycle time	60 s	
Temperature	80°C	
Relative Humidity	Anode/Cathode 100/100%	
Fuel/Oxidant	Hydrogen/N_2	
Pressure	150 kPa absolute	
Metric	**Frequency**	**Target**
Catalytic Activity*	Beginning and End of Life	≤60% loss of initial catalytic activity
Polarization curve from 0 to ≥1.5 A/cm^2**	After 0, 1k, 5k, 10k, and 30k cycles	≤30mV loss at 0.8 A/cm^2
ECSA/Cyclic Voltammetry	After 1, 10, 30, 100, 300, 1000, 3000 cycles and every 5000 cycles thereafter	≤40% loss of initial area
*Activity in A/mg @ 150kPa abs backpressure at 900mV iR-corrected on H_2/O_2, 100%RH, 80°C		
** Polarization curve per USFCC "Single Cell Test Protocol" Section A6		

Table 2
Catalyst Support Cycle and Metrics

Cycle	Hold at 1.2 V for 24h; run polarization curve and ECSA; repeat for total 200h. Single cell 25 - 50 cm^2	
Total time	Continuous operation for 200 h	
Diagnostic frequency	24 h	
Temperature	95°C	
Relative Humidity	Anode/Cathode 80/80%	
Fuel/Oxidant	Hydrogen/Nitrogen	
Pressure	150 kPa absolute	
Metric	**Frequency**	**Target**
CO_2 release	On-line	**<10% mass loss**
Catalytic Activity*	Every 24 h	≤60% loss of initial catalytic activity
Polarization curve from 0 to ≥1.5 A/cm^{2**}	Every 24 h	≤30mV loss at 1.5 A/cm^2 or rated power
ECSA/Cyclic Voltammetry	Every 24 h	≤40% loss of initial area
*Activity in A/mg @ 150kPa abs backpressure at 900mV iR-corrected on H_2/O_2, 100%RH, 80°C		
**Polarization curve per USFCC "Single Cell Test Protocol" Section A6		

Table 3
MEA Chemical Stability and Metrics

Test Condition	**Steady state OCV, single cell 25 - 50cm^2**	
Total time	200 h	
Temperature	90°C	
Relative Humidity	Anode/Cathode 30/30%	
Fuel/Oxidant	Hydrogen/Air at stoics of 10/10 at 0.2 A/cm^2 equivalent flow	
Pressure, inlet kPa abs (bara)	Anode 250 (2.5), Cathode 200 (2.0)	
Metric	**Frequency**	**Target**
F^- release or equivalent for non-fluorine membranes	At least every 24 h	No target – for monitoring
Hydrogen Crossover (mA/cm^2)*	Every 24 h	≤20 mA/cm^2
OCV	Continuous	≤20% loss in OCV
High-frequency resistance	Every 24 h at 0.2 A/cm^2	No target – for monitoring
*Crossover current per USFCC "Single Cell Test Protocol" Section A3-2, electrochemical hydrogen crossover method		

Table 4
Membrane Mechanical Cycle and Metrics
(Test using a MEA)

Cycle	**Cycle 0% RH (2 min) to 90°C dewpoint (2 min), single cell 25 - 50cm²**	
Total time	Until crossover >10 sccm or 20,000 cycles	
Temperature	80°C	
Relative Humidity	Cycle from 0% RH (2 min) to 90°C dewpoint (2 min)	
Fuel/Oxidant	Air/Air at 2 slpm on both sides	
Pressure	Ambient or no back-pressure	
Metric	**Frequency**	**Target**
Crossover*	Every 24 h	≤10 sccm

*Crossover per USFCC "Single Cell Test Protocol" Section A3-1, pressure test method with 3 psig N_2

Excerpts from: **USFCC Single Cell Test Protocol July 13, 2006**
(http://www.usfcc.com/resources/technicalproducts.html#form)

Section A3) Leak Testing

Step one, Pressure Test Method is required. The Electrochemical Hydrogen Crossover Method, Step 2 can be performed in addition to Step 1 for comparison, but is not required.

1) Pressure Test Method: Refer to Leak Check Procedure, Single Cell, USFCC Document Number 04-070 using the pressure settings outlined below,

a) External leaks:

i) Check for sealing leaks using equal 25 psig N_2 on the anode and cathode.

ii) With cell pressurized and gas inlet/exits blocked, a leak is determined when gas pressure drops 1 psi over 10 minutes.

b) Crossover leaks:

i) Check for crossover leaks from anode-to-cathode and cathode-to-anode using 3 psig N_2 on the anode and cathode, respectively (*This point was reworded for clarification.*)

2) Electrochemical Hydrogen Crossover Method:

The testing procedure for hydrogen crossover is based on an electrochemical detection of the molecular hydrogen passing through the membrane. For that purpose, the assembled cell is purged with hydrogen at the anode side and with nitrogen at the cathode side. In this mode, the fuel cell anode serves as reference and counter electrode and the fuel cell cathode acts as the working electrode (three-electrode arrangement). Under these conditions, a voltammogram is recorded. The detected current resulting from the oxidation of molecular hydrogen at the fuel cell cathode is determined.

a) Recommended Equipment:

i) The following equipment is recommended. Equivalent may be used. Record manufacturer, model and settings for actual equipment used.

ii) Princeton Applied Research Potentiostat/Galvanostat, Model 273

b) Assembled Cell Operating Condition:

i) Cell temperature approximately 24°C (room temperature)

ii) Gases at 100% relative humidity

iii) Stoichiometry Hydrogen = 1.5 @ 1 A/cm

iv) (Alternative: 4% Hydrogen/Nitrogen, 500 cc/min)

v) Nitrogen = 30 nl/h

vi) Pressure = 1 bar at sea level.

c) Testing Procedure for Probing the Cathode:

i) Purge the anode with hydrogen and the cathode with nitrogen for at least 30 minutes to equilibrate the cell.

ii) Set the range on the potentiostat to 0.1 to 0.4V and the scan rate to 2.0 mV/s.

iii) Run the scan and wait 10 minutes

iv) Repeat the Sweep Voltammetry.

v) The crossover current is determined from the steady state value at 300 mV. The recorded value is then translated into a hydrogen crossover in terms of ml/min-cm^2.

vi) Repeat the procedure twice to verify the result.

d) Potentiostat settings:

i) Current range: 2 Amps

ii) 1st potential: 100 mV

iii) 2nd potential: 400 mV

iv) Scan speed: 2 mV/s

e) Reference Values

i) The typical acceptable value for hydrogen crossover for Nafion 1135 membrane is 0.014 mL/min-cm^2, which is equivalent to 2 mA/cm^2; see Figure A2 (*not included here*).

Section A6) Polarization Curve Conditions and Load Sequence

a) General Procedure ***(repeated polarizations as described in i and v below are not necessary for the purposes of the DOE Accelerated Stress Test protocol.)***

i) Perform Polarization Curve 1 three times. Then perform Polarization Curve 2 three times.

ii) Table A3 specifies the polarization curve load sequence, to be followed in the order presented.

iii) Maintain conditions for each sequence step for 20 minutes.

iv) A wait period of 10 minutes should be observed between polarization curves. During this period, return the gas flow rates to the equivalent of 10 stoich at 10 amps and set the current to 40 amps.

v) Conduct subsequent polarization curves until repeatable results are observed (within 5mV deviation of the previous polarization curve at 40A). Then record the next three polarization curves as reportable data.

Sequence Step	Current Density (mA/cm^2)
0	0 (use flows for Step 1)
1	100
2	200
3	400
4	600
5	800
6	1000
7	1200

Table A3: Round-Robin Polarization Curve Sequence

b) Polarization Curve 1

i) Polarization Curve 1 test conditions are listed below.

Fuel: Hydrogen, 1.2 Stoich, 100 % RH

Oxidant: Air, 2.0 Stoich, 100 % RH

Temperature (C): 80

Pressures (psig): 25

c) Polarization Curve 2

Polarization test conditions are listed below.

Fuel: Hydrogen, 1.2 Stoich, 100 % RH

Oxidant: Air, 2.0 Stoich, 100 % RH

Temperature (C): 60

Pressures (psig): 0 at outlet (~3psig back-pressure at full flow)

Appendix E: Results from replicated tests

Test 1 replicate:

Figure 40 shows one hour of the current ageing process at four different stages for the replicate of test 1. The drop in OCV after 70 hours indicates pinhole formation.

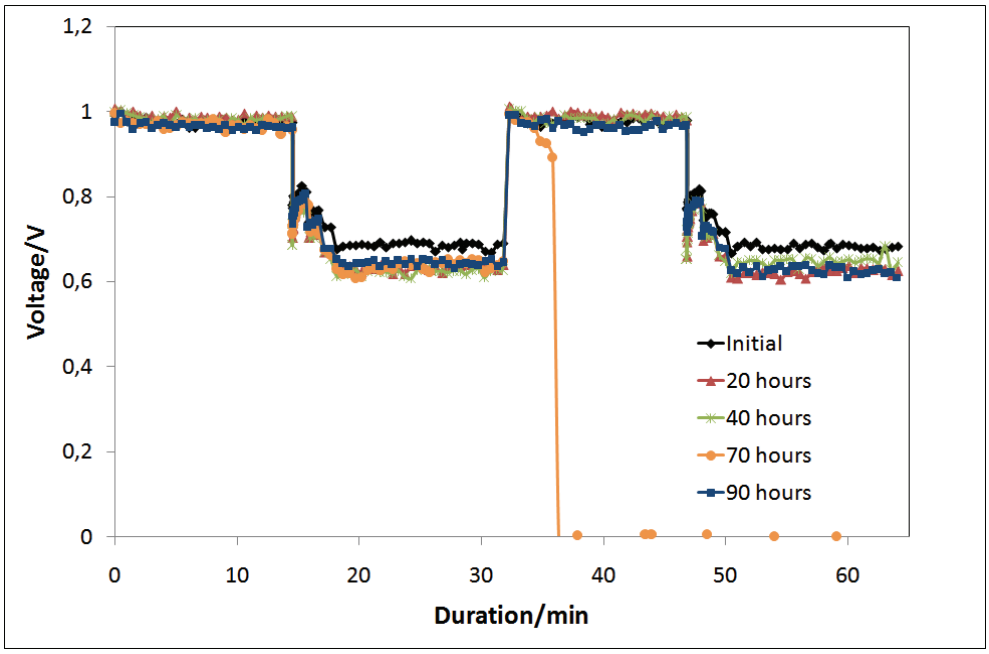

Figure 40 Voltage profile of test 1 replicate, showing 1 hour of the current ageing process at four different stages.

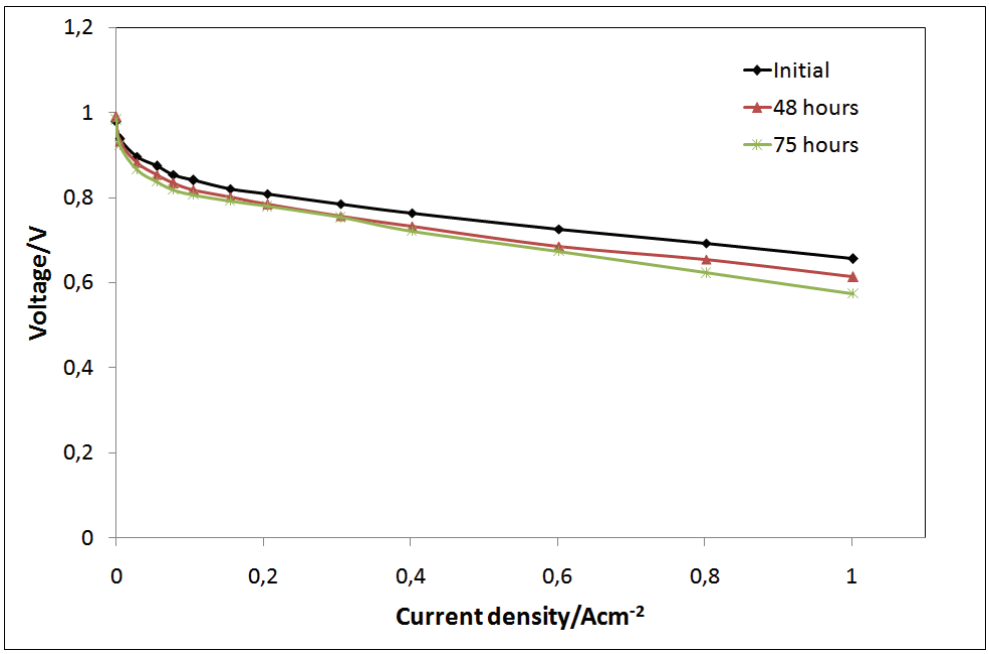

Figure 41 Polarization measurements for replicate of test 1.

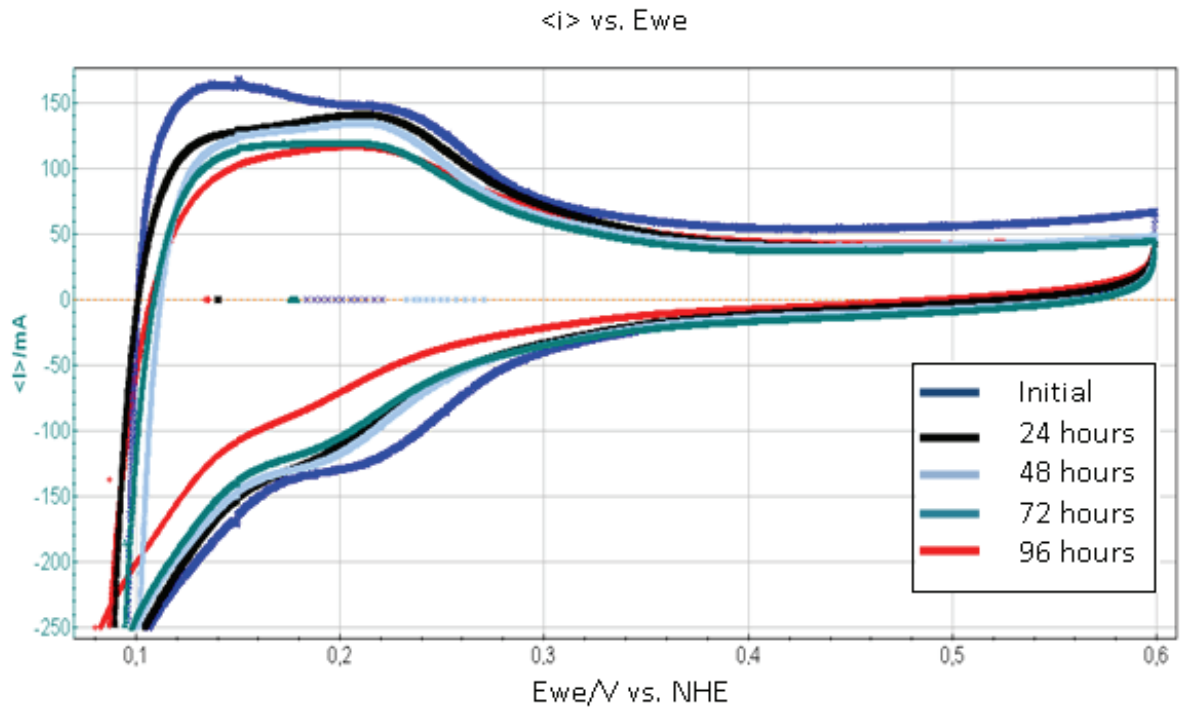

Figure 42 Cyclic voltammetry measurements for replicate test 1 showing a reduction of active area with time.

Test 3 replicate:

Figure 43 shows the voltage profile for the replicate of Test 3. As Test 3 the most significant drop in performance is during the first 100 hours.

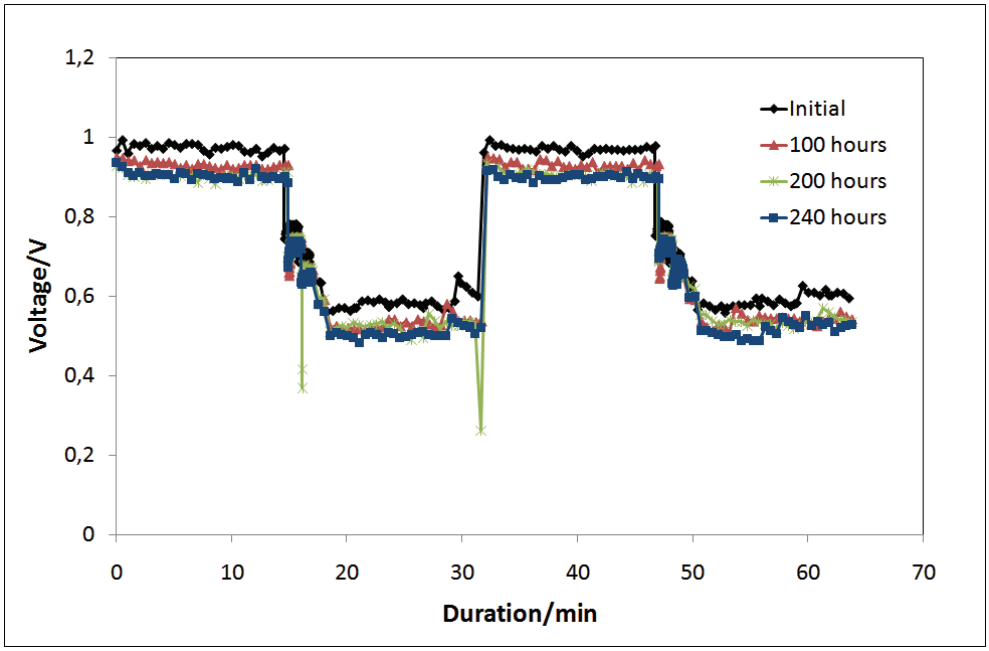

Figure 43 Voltage profile of test 3 replicate, showing 1 hour of the current ageing process at four different stages.

Appendix F: Data from water samples

Water samples from Test 1. (23.04.2008-03.05.2008)						
Sample no.	*Start*	*Stop*	*Duration/h*	*Weight, cathode [g]*	*Weight, anode [g]*	*Remarks*
1	23.04.2008 13:45	23.04.2008 20:50	7.08	79.1522	7.3773	Break-in procedure
2	23.04.2008 20:50	24.04.2008 16:40	19.83	22.5173	6.2403	
3	24.04.2008 16:40	25.04.2008 20:45	28.08	32.0485	10.0724	
4	25.04.2008 20:45	28.04.2008 08:45	60.00	44.3977	14.5925	Emergency on. Stop 27.04.08 ca.kl.1100.
5	28.04.2008 08:45	29.04.2008 10:43	25.97	30.9828	9.8239	
6	29.04.2008 10:33	30.04.2008 10:15	23.70	28.4076	9.6532	
7	30.04.2008 10:15	01.05.2008 13:25	27.17	28.9776	9.4525	
8	01.05.2008 13:25	02.05.2008 12:30	23.08	27.6557	9.8691	
9	02.05.2008 12:30	03.05.2008 14:40	26.17	12.5755	12.5655	
10	03.05.2008 14:40	04.05.2008 11:55	21.25	8.8873	3.8976	

Table 10 Data from water samples test 1.

Water samples from Test 2. (25.05.2008-27.05.2008)						
Sample no.	*Start*	*Stop*	*Duration/h*	*Weight, cathode [g]*	*Weight, anode [g]*	*Remarks*
1	*25.05.2008 16:20*	*25.05.2008 23:40*	*7.33*	*68.0141*	*7.1568*	Break-in procedure
2	*25.05.2008 23:40*	*26.05.2008 15:41*	*16.02*	*18.6566*	*2.596*	
3	*26.05.2008 15:41*	*27.05.2008 15:07*	*23.43*	*17.2376*	*4.2082*	Several stops during this cycle.
4	*27.05.2008 15:07*	*27.05.2008 16:40*	*1.55*	*6.5193*	*0.5002*	Stop.

Table 11 Data from water samples test 2.

Water samples from Test 3. (20.03.2008-01.04.2008)						
Sample no.	*Start*	*Stop*	*Duration/h*	*Weight, cathode [g]*	*Weight, anode [g]*	*Remarks*
1	20.03.2008 12:55	20.03.2008 18:10	5.25	45.163	9.1745	Break-in procedure
2	20.03.2008 18:10	21.03.2008 17:15	23.08	109.2446	30.741	
3	21.03.2008 17:15	23.03.2008 10:47	41.53	136.467	54.8937	Stop resulting in extra OCV time (16 hours extra OCV)
4	23.03.2008 10:47	24.03.2008 11:07	24.33	118.8225	31.5095	
5	24.03.2008 11:07	25.03.2008 11:31	24.40	117.0255	31.2515	
6	25.03.2008 11:31	26.03.2008 12:00	24.48	118.5307	30.5914	
7	26.03.2008 12:00	27.03.2008 12:30	24.50	118.5469	31.3554	
8	27.03.2008 12:30	29.03.2008 09:34	45.07	137.2226	33.9786	Stop resulting in extra OCV time.
9	29.03.2008 09:34	30.03.2008 11:06	25.53	119.7061	30.1679	
10	30.03.2008 11:06	31.03.2008 11:22	24.27	117.7083	30.7537	
11	31.03.2008 11:22	01.04.2008 12:11	24.82	112.3704	27.4022	

Table 12 Data from water samples test 3.

Water samples from Test 4. (13.05.2008-22.05.2008)						
Sample no.	*Start*	*Stop*	*Duration/h*	*Weight, cathode [g]*	*Weight, anode [g]*	*Remarks*
1	13.05.2008 12:05	13.05.2008 19:45	7.67	56.0895	5.0834	
2	13.05.2008 19:45	14.05.2008 17:04	21.32	52.9587	5.698	
3	14.05.2008 17:04	15.05.2008 18:11	25.12	59.7575	8.4115	
4	15.05.2008 18:11	16.05.2008 17:30	23.32	56.2237	7.881	
5	16.05.2008 17:30	18.05.2008 13:11	43.68	103.2551	15.0619	2 days of duration
6	18.05.2008 13:11	19.05.2008 15:45	26.57	63.8108	11.8423	
7	19.05.2008 15:45	20.05.2008 17:03	25.30	56.1207	8.5722	
8	20.05.2008 17:03	21.05.2008 19:48	26.75	54.6823	8.7275	
9	21.05.2008 19:48	22.05.2008 15:45	19.95	49.2095	7.614	
10	22.05.2008 15:45	24.05.2008 11:03	43.30	89.8165	12.5623	2 short stops due to BP problems.

Table 13 Data from water samples test 4.

Water samples from Test 3 replicate. (28.05.2008-07.06.2008)						
Sample no.	*Start*	*Stop*	*Duration/h*	*Weight, cathode [g]*	*Weight, anode [g]*	*Remarks*
1	28.05.2008 13:04	28.05.2008 19:00	5.93	50.4881	4.4002	Break-in procedure
2	28.05.2008 19:00	29.05.2008 19:52	24.87	146.7394	23.402	
3	29.05.2008 19:52	31.05.2008 03:04	31.20	175.59	29.4433	
4	31.05.2008 03:04	31.05.2008 17:38	14.57	73.2535	13.6856	
5	31.05.2008 17:38	01.06.2008 20:05	26.45	136.8938	25.4988	
6	01.06.2008 20:05	03.06.2008 08:53	36.80	189.4802	36.3172	
7	03.06.2008 08:53	04.06.2008 08:58	24.08	121.5508	24.9923	
8	04.06.2008 08:58	05.06.2008 08:49	23.85	123.3661	22.8818	
9	05.06.2008 08:49	06.06.2008 09:40	24.85	125.2415	24.7462	
10	06.06.2008 09:40	07.06.2008 17:25	31.75	162.6703	32.4894	

Table 14 Data from water samples replicate test 3